Snow Hydrology in the Netherlands

Developing snowmelt algorithms for Dutch regional water management modules

MSc Internship report

By Doris Wendt
January 2015

Snow Hydrology in the Netherlands

Developing snowmelt algorithms for Dutch regional water management modules

MSc Internship report

Author:
Doris Wendt BSc
Student nr. 19910116939030

Supervised by:
Dr. Ir. R. Hurkmans
HKV Lijn in water

Dr. Ir. A.J. Teuling
Wageningen University and Research centre

Examintor:
Prof. Dr.Ir. R. Uijlenhoet
Wageningen University and Research centre

HWM- 70424

Hydrology and Quantitative Water Management Group

September 2014 – January 2015

Abstract

Almost every winter, Dutch lowlands are covered by a thin layer of snow for several days. Despite its occurrence, this surface storage is currently not included in the regional water management models. Water boards are often surprised by snowfall events, and even more by its melt that results in a sudden peak discharge. Snow storage causes a delay in discharge. Current models have great difficulties to quantify the delayed peak. Hence, the aim of this research is to develop a melt algorithm for Dutch snow conditions in order to include snowmelt in the regional water management models.

By this algorithm, an extra snow reservoir was implemented to the original model. Recorded precipitation was separated for rain and snow. We used snowfall as input for the reservoir, which was depleted by predicted melt. The melt was simulated using three methods: a temperature-index algorithm, a semi-empirical algorithm and an energy balance algorithm. Simulated melt and rainfall were used as input for the original hydrological model.

In this study, two models have been used to test the algorithms (using Sobek and WALRUS), which simulated discharge in the Barneveldse beek and Reusel catchment. Goodness of fit parameters were used to judge upon simulation accuracy. Moreover, a validation set with snow depth observations of the KNMI verified the modelled surface reservoir.

Results show that melt algorithms improve current discharge simulations. Peak discharge is timed better in the simulations, but accuracy of the absolute discharge peak differs per winter. In general, best performances are achieved using the two (semi-) empirical algorithms. The energy balance algorithm seems to be sensitivity to an increase of temperature and vapour pressure. Hence, it is necessary to measure these climate variables correctly.

Acknowledgements

For the completion of my MSc Internship report, I would like to thank Ruud and Ryan, who were my supervisors during this research. I appreciated their support and guidance very much. Thanks to the KNMI, I could to this research, since they share all their snow data on their website and the Water boards ("De Dommel" and "Vallei en Veluwe"), whose data I could use for the case studies.

Finally, I express my warm thanks to some people in special. Their support has been very helpful: Claudia Brauer, Paul Torfs, Regina Hock, Bertus de Graaff, Iris Vreugdenhil, Raymond Loos, Jurriaan ten Broek, Hein Wendt, Irene de Vries, Geerten Horn, Fabian Kemps Verhage, Kawire Gosselink, Loes Masselink, Sara de Heer, Laura Antosch, Théau Dusart and Merel Kooi.

Contents

1. Introduction

Almost every winter, the Dutch lowlands are covered by a thin layer of snow for several days. When snow falls, frozen crystals accumulate on the surface and they store the water for a certain amount of time. If this surface storage melts, the accumulated amount of water will be drained. This sudden peak discharge may surprise water managers, who did not expect the accumulated peak discharge.

Current rainfall-runoff models have great difficulties to quantify this (higher) melt peak. Water boards have the need to predict these peaks accurately, as they cause troubles in the regional water management (Pers. Comm. De Graaf, 2014). In an attempt to adjust the hydrological models for these melt events, water consultants have tried to calibrate discharge for these winters. However, the timing of the runoff peaks remained different to the observations and the peak discharge was not simulated well. Hence, there is a need to extend these hydrological models with snowmelt algorithms.

Melt models are not new, they exist in many forms. Nevertheless, the majority is developed and calibrated on mountainous areas or colder climates (DeWalle and Rango, 2011). The easiest approach for snowmelt simulation is to use a temperature-index algorithm that assumes a certain amount of melt per time step. This model seems to crudely generalize physical processes, although reasonable results are achieved after calibration (Hock, 2003). Attempts to improve this empirical model have also included physical factors as sun radiation and wind speed. These climate variables have a direct relation to snowmelt, although an empirical conversion factor is required to add this component to the temperature-index algorithm (Kustas, et al. 1994). An alternative has developed by Regina Hock, who developed a snowpack energy balance model in order to simulate melt on an hourly basis. The energy balance included all fluxes present in the snowpack by an extensive dataset. An accurate simulation of melt is the result of this model (Hock, 1999).

In contrast to comparable snowmelt studies, only a limited amount of snow data was available for this research, since snowmelt was not simulated previously in the Netherlands. In addition, the required degree of complexity was unknown. In order to develop and test snowmelt algorithms, a specific time frame, the three latest snow rich winters were selected for research. In addition, discharge data was available for two research catchments for which the algorithms could be tested. Using this framework, this research was investigated the possible melt algorithms for Dutch winters.

The aim of the study is to develop melt algorithms for Dutch winters. These algorithms should be applicable for the current regional water management models (e.g. Sobek and WALRUS) and no additional climate data should be required. By this means, the algorithms should work using (already) available information in order to fully support integration of regional water management models and the melt algorithms. The integration is required to product these modules, as this study is a result of the cooperation of Water consultant HKV Lijn in water and the Wageningen University in the context of a MSc Internship.

The outline of the report is built as follows. First the dataset and methods are explained in the next chapter. Consequently, the results of these methods are presented in chapter 3. The outcomes are questioned and discussed in chapter 4. The work is concluded in chapter 5, recommendations can be found in the last chapter.

2. Method

2.1. Data collection

Climate data was available via the site of Royal Netherlands Meteorological Institute (KNMI). KNMI has published daily and hourly records online for 35 automatic weather stations (see Annex A.1). The following climate variables have been recorded; air temperature (T_a in ℃), precipitation (P in mm h^{-1}), wind speed (u in m s^{-1}), global radiation (G in J cm^{-2}), sea level air pressure (E_a in Pa), relative humidity (RH in %) and cloud cover (m_c in octants or fractional).

Some cloud cover records were missing within the studied timeframe (41 records in 2009-2012). Missing observations were related to precipitation events in the same time step. If no rain occurred, gaps were replaced by zero, which implied clear sky conditions. Otherwise full cloud cover was assumed (m_c = 1). The sensitivity of this replacement is discussed in section 3.7.2.

Daily precipitation records (including rain and snow depth) were acquired by the 325 precipitation KNMI stations (see A.2). Rain and snow were collected in unshielded gauges, which were checked by volunteers on daily basis (at 8 a.m.).

Discharge time series were available from previous studies in two catchments. In Barneveld, an acoustic Doppler velocimeter measured the discharge (Jungermann and Graaff 2013)**.** Quality of these measurements has been checked previously in this study. In Reusel, an intervention structure measured discharge at the outlet of the catchment. This structure has been implemented to maintain the water level by movable weirs. The crest level was adjusted to accommodate discharge changes automatically, but instantly. This caused sudden fluctuations in the discharge observations. These small differentiations had been smoothened by a 24hour moving average.

2.2. Snow data from the KNMI

In comparable snow hydrology studies, an extensive dataset has often been used to calibrate the simulated SWE over a certain time (Egli, et al. 2009). Even in commercial settings, HBV models are often updated for the measured snowfall or SWE to correctly simulate discharge in the melt season (Pers. Comm. NVE, March 2014). Dutch snow conditions may not vary in such extent, although some measurements are required to validate model results.

This validation set was generated using KNMI snow depth measurements. Daily snow depth observations outlined a fine network of point-wise measurements. However, these measurements are less representative on smaller scales (e.g. catchment level) (Goudenhoofdt and DeLobbe, 2009). Therefore, interpolation was applied, which conceptualized an average snowy winter in the Netherlands. In general, the little spatial dependency of snowfall complicates the interpolation. Wind may redistribute snow particles (drift) after the snow event. Moreover, an irregular pattern may be formed by obstacles in the landscape (e.g. trees, buildings). The spatial structure of Dutch snowpacks would already be less complex compared to non-mountainous regions (e.g. absence of large elevation, orientation or slope differences) (Erxleben, et al. 2002).

Reasoning that the spatial structure of snowfall is less than the spatial continuity of rainfall, a simple deterministic interpolation (e.g. Thiessen Polygons) would have a lower predictive capacity (Erxleben, et al. 2002). In addition, the gradient of observations would be neglected. More comprehensive methods would increase this predictive power. Commonly used to interpolate rainfall is the inverse distance weighted interpolation (IDW) (Klopstra and Versteeg 2005; Heijkers et al. 2011; Versteeg et al. 2012). IDW uses a non-linear equation to increase weights for observations close to a grid cell (Watson and

Philip, 1985). The powers for the equation are adjustable and had to be set first (Ly, et al. 2013). Within the range of accuracy, the chosen power for the interpolation function would not increase interpolation errors significantly for snowfall (Dirks, et al. 1998; Graysol and Bloschl, 2001).
In fact, spatial variability of snow would be better understood using a geostatistical interpolation. Ordinary kriging is often used to interpolate snowfall (Erxleben, et al. 2002). Predictions are improved compared to other methods and a range of certainty and accuracy is given (Hosang and Dettwiler, 1991). By including the covariance, the spatial structure of the data is built in the interpolation method (Ly, et al. 2013; Matheron, 1971). Even better results would be achieved if binary regression tree had been combined with kriging (Erxleben, et al. 2002). However, this interpolation method was undesirable due to data availability. Erxleben, et al. (2002) emphasises that interpolation optimization goes up to 70 per cent; the complexity of snow distribution is too large to be fully predicted.
On forehand of kriging, a variogram is made to detect the autocorrelation of the dataset. In a variogram, different models can be used (e.g. exponential, spherical, Gaussian, rational quadratic). A suitable model was chosen using the best fit by minimizing the sum of least squares.

2.3. Conversion of snow depth to snow water equivalent

The validation set was completed by the conversion of snow depth to snow water equivalent (SWE). SWE was computed by the snow density (see equation 20). Fortunately, a few local measurements were carried out to verify the theoretical density. Hence, literature had been used to define a range of suitable conversions rates.

$$SWE = h_s \frac{\rho_s}{\rho_w}$$

Equation 1: Snow Water Equivalent (SWE in cm) is related to the snow depth (h_s in cm), snow density (ρ_s) and density of water (ρ_s) both measured in g cm^{-3}.

Variable ranges of snow density are reported by snow hydrology studies. These ranges varied mostly per climate region. According to the paper of Sturm, et al. (2010) SWE can be determined by an algorithm based on specific climate classes. These classes were specifically set for the snow cover characteristics in a region and therefore these classes might differ from the climate classes' scheme of Köppen (1924). Dutch snow cover characteristics would be classified according to the maritime climate map, even though time series analyses indicated the Dutch conditions in between two climate classes (ephemeral and maritime) (Sturm, et al. 1995). Since measurements were absent in this research phase, typical values of the maritime climate have been selected. General density values included the average ± standard deviation, which have been deducted from approx. 8220 measurements (Sturm, et al. 2010).
Local data was collected during a short snow event in Wageningen at 26th and 27th December 2014. A full snow cover was observed for two days, and 6 density measurements were done at approximately 12:00p.m. Density was measured by the weight of a fixed volume (1L) of snow at 6 locations all close to the University (within the scale of 1 km^2).

2.4. Snowfall-rainfall partitioning

In a typical Dutch winter, air temperature fluctuates from −5 to 10℃ (KNMI data). Within this range, precipitation can either fall as rain (P_r) or snow (P_s). Separation of the two was done using a temperature threshold. In reality, multiple processes in the atmosphere determine the type of precipitation, although air temperature is a commonly used variable to distinguish two kinds (Kienzle, 2008; Loth, et al. 1993; Thériault, et al. 2012).

A static temperature threshold (T_{snow}) is a first and simple approach. In this case, 100% snowfall is assumed for temperatures below the threshold (see equation 1**)**. Despite its simplicity, this approach has been applied intensively in many water management models, e.g. the Swedish HBV model (Bergstrom, 1995).

$$P_s = P \qquad T_a < T_{snow}$$
$$P_r = P \qquad T_a \geq T_{snow}$$

Equation 2: Static threshold temperature model. If air temperatures (T_a) are below the threshold (T_{snow}), 100% snow (P_s) is assumed. If T_a exceeds T_{snow} precipitation (P) is assumed to be rain (P_r).

Secondly, a dynamic threshold is introduced by Pipes and Quick (1976) (further abbreviated as dynamic PQ model). They proposed a gradual change in the proportion rain and snow. The proportion is determined by the measured maximum and minimum air temperature for which snow fell (T_{min} =0.6℃ and T_{max} =3.6℃) (see equation 2). This gradual shift in precipitation is part of a larger model to simulate stream flow in mountain basins. For model characteristics see Kienzle (2008) or Pipes and Quick (1976).

$$P_s = P \qquad T_a \leq T_{min}$$
$$P_r = \frac{T_a}{3} - 0.2 \qquad T_{min} < T_a < T_{max}$$
$$P_r = P \qquad T_a \geq T_{max}$$

Equation 3: Dynamic threshold temperature model by Pipes & Quick (1977). Rain and snow separation works similarly to the static threshold temperature model (Equation 1). Only a gradual change is added for T_a between minimum and maximum threshold temperature (T_{min} and T_{max}).

The third method is used by the variable infiltration capacity model (VIC). VIC can be classified as a distributed soil-vegetation-atmosphere transfer model (Liang, et al. 1994), and has been developed for large-scale applications and various river basins globally. In the VIC snow model, a proportional change of precipitation was defined by linear interpolation of the temperature and the total precipitation (see equation 3) (Andreadis, 2009). This approach is therefore slightly different than the dynamic threshold of PQ (described previously). In addition, somewhat different thresholds are also applied: T_{min} =$-0.5^{\circ}C$ and T_{max} =$1.5^{\circ}C$.

$$P_s = P \qquad T_a \leq T_{min}$$
$$P_s = \frac{T_{max} - T_a}{T_{max} - T_{min}} P \qquad T_{min} < T_a < T_{max}$$
$$P_r = P \qquad T_a \geq T_{max}$$

Equation 4: Dynamic threshold temperature model by VIC model (Andreadis, 2009). Snow and rain are separated similarly to the static threshold model (Equation 1). The precipitation between the thresholds is divided by a linear interpolation according to the minimum and maximum threshold temperature (T_{min} and T_{max}).

We have tested all three methods for the selected winters in 2009-2012. In the result section, their performance is shown, just as the validation with the snow depth observations of the KNMI.

2.5. Snowmelt pre-processors

The calculated amount of snow was used as input for the snowmelt algorithms. Snowfall was calculated as snow water equivalent (SWE in mm). The SWE storage is seen as a surface reservoir, which is depleted by snowmelt. Logically, no more melt can occur than is stored in the reservoir.
These simple, but essential steps were modelled in the developed algorithms, which were refined to simulate melt from shallow snowpacks in lowlands (tested in the Netherlands).
Modelling snowmelt urged understanding of physical processes during snowmelt. In principle, melt is a phase change of water. Phase changes involve different rates of energy exchange (see table 1). For instance, less energy is required for melting than for sublimation (8.3 times less). The signs in table 1 refer to either incoming energy sources (positive) or outgoing energy fluxes (negative), taking the surface as a reference level. This terminology is commonly used in glaciology. (Hock, 1999; DeWalle and Rango 2011)

Table 1: Phase change of water (DeWalle and Rango 2011)

Phase change	**Process**	**Energy exchanged** @ 0 in ℃ (MJ kg^{-1})	
Vapour to Liquid	Condensation	Latent heat of vaporization	−2.50
Liquid to Vapour	Evaporation	Latent heat of vaporization	+2.50
Liquid to Solid	Freezing	Latent heat of fusion	−0.33
Solid to Liquid	Melting	Latent heat of fusion	+0.33
Solid to/from Vapour	Sublimation	Latent heat of sublimation	±2.84

2.6. Snowmelt models

Snowmelt has yet not been included in regional hydrological models in the Netherlands. Therefore it was unknown, which degree of complexity is required to model snowmelt accurately on this scale. A comprehensive investigation could be done by the available climate data and finally, we have developed three melt models. First, the method of two (semi-)empirical algorithms is explained, which is followed by an extensive energy balance algorithm to simulate major energy fluxes in a snowpack.

2.6.1. Temperature-index algorithms

Temperature-index algorithms are extensively used to model snowmelt in foreign hydrological models (e.g. the HBV model). This concept assumes that physical processes that cause snowmelt are positively related to temperature. Consequently, snowmelt can be predicted by using temperature only, although the empirical factor may require calibration to local conditions (Hock, 2003).

Commonly known is the degree-day approach, which uses an empirical factor to predict snow or ice melt. A wide range of empirical values is reported by various authors, since this degree-day factor requires calibration to simulate melt accurately. Daily values vary from 3.2-9.0 mm d^{-1} (Kustas, et al. 1994; Hock, 2003).
However, hourly melt factors had to be used for these algorithms. The hydrological models used in this study, forced this time scale to the pre-processors. Therefore, the degree-*hour* factor (DHF) was set on 0.32 mm h^{-1} ℃$^{-1}$. This value was based on the work of Pellicciotti, et al. (2005). Moreover, DHF agreed with the suggested range of SWAP in Kroes, et al. (2008), Kustas, et al. (1994) and Hock (2003). The threshold for melting conditions (T_{ref}) was set on 0.5℃ (Hock, 2003) (see equation 4).

$$M_{DHF} = \begin{cases} DHF\,(T_a - T_{ref}) & T_a > T_{ref} \\ 0 & T_a \leq T_{ref} \end{cases}$$

Equation 5: Melt rate (M_{DHF} in mm h^{-1}) predicted by the degree-hour factor (DHF in mm h^{-1} ℃$^{-1}$) for the hours that $T_a > T_{ref}$ (threshold for air temperature in ℃).

The melt rate can be related to more elements than only temperature. Many authors have attempted to improve this temperature-index model by including radiation, vapour pressure or wind speed (Hock, 2003). On hourly time scales, a shortwave radiation balance was added to the standard model by Pellicciotti, et al. (2005). Their best fit has been used for our second pre-processor (see equation 5). Similar to the previous model, a temperature factor was included (TF equals 0.05 mm h^{-1} ℃$^{-1}$). The shortwave radiation factor was defined on 0.0014 m ^{2}mm $W^{-1}h^{-1}$ ℃$^{-1}$. Incoming shortwave radiation (G in W m^{-2}) was measured, but the reflected component is also determined by the albedo (α). The albedo ranged from 0.5-0.9 in various studies (Paterson, 1994; Kustas, et al. 1994; Hock, 1999; DeWalle and Rango 2011). Even though albedo may vary quickly, a constant value was assumed for this study. Simply fresh snow was simulated by an albedo of 0.7 (Brock, 2000; Hock 2014). T_{ref} is kept constant in both snowmelt algorithms.

$$M_{SRF} = \begin{cases} [TF + SRF\,(1-\alpha)G]\,[T_a - T_{ref}] & T_a > T_{ref} \\ 0 & T_a \leq T_{ref} \end{cases}$$

Equation 6: Melt rate (M_{SRF} in mmh^{-1}) predicted by the temperature factor (TF in mmh^{-1} ℃$^{-1}$), shortwave radiation factor (SRF in m^2mm$W^{-1}h^{-1}$ ℃$^{-1}$) times the shortwave radiation balance (W/m^2) for the hours that $T_a > T_{ref}$ (both measured in ℃).

Both modules are generally accepted as good melt indicators in other study areas (Pellicciotti, et al. 2005; DeWalle and Rango 2011; Hock, 2003). However, Dutch winters may differ from these case studies. In the Netherlands, winters are often cloudy and wet. Rain-on-snow events may have a crucial influence on the Dutch melt rates. We have designed an alternative to the temperature-index models in order to include the energy fluxes during precipitation events. Therefore, the third pre-processor involved a comprehensive algorithm: the energy balance.

2.6.2. Energy balance algorithm

Energy fluxes affecting snowpack melt have been modelled extensively by the energy balance. The balance is defined as the sum of the energy fluxes at the snow surface (T_s = 0℃). Six fluxes together determine the energy balance: melt energy (Q_M), net radiation (Q_N), sensible heat flux (Q_H), latent heat flux (Q_L), ground heat flux (Q_G), and the sensible heat flux of rain (Q_R) (see equation 6). (Hock, 1999; 2014)

$$Q_M = Q_N + Q_L + Q_H + Q_G + Q_R$$

Equation 7: Surface Energy balance by Hock (1999). The energy available for melt (Q_M) is computed by the sum of net radiation (Q_R), latent heat flux (Q_L), sensible heat flux (Q_H), ground heat flux (Q_G) and the sensible heat flux of rain (Q_R). All fluxes are measured in Wm^{-2}.

Not all these components have an equal share to the melt events. As in many natural balances, radiation of the sun is a principal incoming source of energy. This element is defined by Q_N, which represents the balance between shortwave (G (1-α)) and longwave (Ln) radiation (see equation 7). On clear-sky days, incoming shortwave (or global) radiation contributes the majority of the melt energy.
Global radiation was measured by automatic weather stations of the KNMI, which records showed a diffused signal due to the cloud cover. Hence, shortwave radiation had a relatively little share in this study compared to other researched areas (Sicart et al. 2008; Chen et al., 2011; Hock, 1999).

$$Q_N = G\,(1-\alpha) + Ln$$

Equation 8: Net radiation (Q_N) is the balance of global radiation (G) minus the reflected share due to the albedo (α), plus the longwave radiation balance (Ln). All fluxes are expressed in Wm^{-2}.

Clouds affect both shortwave and longwave radiation. An important feedback mechanism is the clouds' isolation layer on the surface. Longwave radiation emitted by the atmosphere can no longer be released and accumulates under the cloud cover. Hence, this flux increases and may become an important source for melt (Hock, 1999; Juszak and Pellicotti, 2013).
Longwave radiation is parameterized in multiple ways (Juszak and Pellicotti, 2013), although we chose to use a simplified method by Kustas, et al. (1994) and DeWalle and Rango (2011). The net longwave flux is described in equation 8 (Kustas, et al. 1994; Brutsaert, 1975).

$$Ln = \varepsilon\,\sigma\,(\varepsilon_{skyo}(1 + c\,m_c^2)\,T_{aK}^4 - T_{sK}^4)$$

Equation 9: Longwave radiation flux defined by Kustas, et al. (1994) and Brutsaert (1975). The outgoing flux is specified by the surface temperature (T_{sK} in Kelvin), surface emissivity (ε, dimensionless) and Stefan-Boltzmann's constant (σ in $Wm^{-2}K^{-4}$). Incoming longwave radiation is a function of the atmospheric emissivity (ε_{skyo}, dimensionless), and air temperature (T_{aK} in Kelvin).

Outgoing longwave radiation is specified by surface temperature (T_{sK} = 273.15K), surface emissivity (ε = 0.985) and Stefan-Boltzmann's constant (σ = 5.67E−8 W m^{-2} K^{-4}). Incoming longwave radiation depends

on the atmospheric emissivity (ε_{skyo}), and air temperature (T_{aK} in Kelvin). Atmospheric emissivity is determined by the effective atmospheric emissivity under clear skies and its correction for the fractional cloud cover (Kustas, et al. 1994). This method differs slightly from more recent defined versions (Marty and Philipona, 2000; Juszak and Pellicotti, 2013) (ε_{skyo} described in equation 9).

$$\varepsilon_{skyo} = 0.642\ (e_a/T_a)^{1/7}$$

Equation 10: Effective atmospheric emissivity under clear sky conditions defined by vapour pressure (e_a) and air temperature (T_a) (Kustas, et al. 1994; Brutsaert, 1975; DeWalle and Rango 2011)

The effective atmospheric emissivity computation was completed with the vapour pressure (e_a in Pa) that was calculated in equation 10 from the saturated vapour pressure above ice (e_{sat} in Pa) and the relative humidity (RH in %) (KNMI 2000:67).

$$e_a = RH\ 6.112\ e^{(22.46\ T_{aK}\ /(T_{aK}+272.62))}$$

Equation 11: Vapour pressure (e_a) determined by the relative humidity (RH), saturated vapour pressure above ice as a function of air temperature in Kelvin (T_{aK}) (KNMI 2000).

Turbulent fluxes are the other principal fluxes in the energy balance. These fluxes are defined by humidity and temperature gradients between surface and lower parts of the atmosphere. Determining factors were wind speed (u in ms^{-1}) and bulk coefficient of vapour exchange (C_{en}, dimensionless) in the following equations (equation 11 and 13).

$$Q_L = (\rho_a 0.622\ L_v\ /p_a)\ C_{en}\ u\ (e_a - e_0)$$

Equation 12: Latent heat flux (Wm^{-2}) computed by air density (ρ_a in kg m^{-3}), latent heat of vaporisation (L_v in J kg^{-1}), total atmospheric pressure (p_a in 1E5 Pa), bulk transfer coefficient for vapour exchange in neutral stability (C_{en}, dimensionless), wind speed (u in m s^{-1}) and the difference of surface and atmospheric vapour pressure (e_a-e_0 both in Pa).

Latent heat (Q_L) is defined by the density of air (ρ_a = 1.29 kg m^{-3} at 0℃), latent heat of vaporisation (L_v = 2.49E6 J kg^{-1}), total atmospheric pressure (p_a in 1E5 Pa), bulk transfer coefficient for vapour exchange (C_{en}, dimensionless), wind speed (u in m s^{-1}), atmospheric vapour pressure (e_a in Pa at height z), and the vapour pressure at snowpack surface (e_0 in 610.78 Pa). A snowpack surface of 0℃ was assumed for the computation of e_0. Vapour pressure was defined for the height of the meteorological station (z = 1.5m). We used this height for the aerodynamic roughness length indices. Additionally, the height defined also the C_{en} in neutral stability (see equation 12)

$$C_{en} = k^2[\ln(z\ z_0^{-1})]^{-2}$$

Equation 13: Bulk transfer coefficient of vapour exchange (C_{en}, dimensionless) determined by the von Karmin constant (k, dimensionless), height of meteorological station (z in m) and the surface roughness (z_0 in m).

A surface roughness value was assumed for the fallen snowpack, as these characteristics are unknown for a typical Dutch snow cover. A typical smooth value was chosen (z_0 is 0.0005m) (DeWalle and Rango 2011).

The sensible heat flux was calculated similarly to the latent heat flux (see equation 13). The flux is defined by the difference in air and surface temperature, wind speed, bulk transfer coefficient for sensible heat for neutral stability (C_{hn}, dimensionless), specific heat of air (1005 J kg^{-1} K^{-1}) and the density of air.

$$Q_H = \rho_a c_p \, C_{hn} u (T_{aK} - T_{sK})$$

Equation 14: Sensible heat flux (Q_H in W m^{-2}) defined by air density (ρ_a in kg m^{-3}), specific heat of air (c_p in J kg^{-1} K^{-1}), bulk transfer coefficient for sensible heat for neutral stability (C_{hn}, dimensionless),wind speed (m s^{-1}), and the difference of air and surface temperature (T_{aK} - T_{sK} both in Kelvin).

Bulk transfer coefficients for both turbulent fluxes were assumed to be equal. The Bowen ratio is thereby simplified to a dimensionless ratio β: $\beta = Q_H / Q_L$ (DeWalle and Rango 2011).

The two remaining fluxes have only a little share in the energy balance. The ground heat flux represents temperature gradients in the snowpack and the thermal conductivity (k_g in W m^{-1} ℃$^{-1}$) (see equation 14).

$$Q_G = k_g \frac{\partial T_g}{\partial z_s}$$

Equation 15: Ground heat flux (Q_G in W m^{-2}) computed by the temperature gradient (δT_g in ℃$^{-1}$ and δz_s in m) in the snowpack and the thermal conductivity (k_g in W m^{-1} ℃$^{-1}$)

Particularly in moderate climates, the snow cover can be relatively shallow and temperate (cold content is equal to 0℃) (Hock, 1999; Sturm, et al. 1995). Therefore, the ground heat flux would be of marginal influence in the Dutch case studies, and Q_g was assumed to be zero.
The last flux of the energy balance is the sensible heat flux of rain (see equation 15). The sensible heat flux is determined by the rainfall intensity (P_r in m s^{-1}), density of water (ρ_w = 1000 kg m^{-3}), specific heat of liquid water (c_w = 4.18E3 J kg^{-1} ℃$^{-1}$), and the difference of rain temperature (T_a=T_r) and snow temperature (0℃) (DeWalle and Rango 2011).

$$Q_R = P_r \, \rho_w \, c_w (T_r - T_s)$$

Equation 16: Sensible heat flux of rain (Q_R in W m^{-2}) determined by the rainfall intensity (P_r m s^{-1}) , water density(ρ_w kg m^{-3}), specific heat (c_w in J kg^{-1} ℃$^{-1}$), and the temperature difference of rain (T_r) and snow (T_s) both in ℃.

In essence, a warm incoming volume of rain would be a minor contributor to snowmelt. However, rain-on-snow can accelerate feedback processes, which caused large melt events previously (Marks, et al. 1998; 2001). Latent and sensible heat fluxes supply a lot of energy to the snowpack during a precipitation event, due to high wind speeds and high humidity rates. Conversely, shortwave radiation is negatively affected during these events. Clouds limit global radiation, although the albedo becomes less due to a change in colour. (Hock, et al. 1999; Marks, et al. 1998; DeWalle and Rango 2011)
Finally, the available energy for snowmelt (Q_M) was found by the sum of all these fluxes (equation 6). Energy conversion is done using the density of water and the latent heat of fusion (L_f = 0.334E6 J kg^{-1}) (see equation 16) (DeWalle and Rango 2011). The thermal quality of a snowpack is thus neglected. Thermal quality incorporates the liquid-water content in snow, but in this study there was no information available about the liquid-water content of the last snow events in the Netherlands.

$$M_{EB} = Q_M \left(\rho_w \, L_f\right)^{-1}$$

Equation 17: Melt rate (M_{EB} in mm h^{-1}) according to the available melt energy (Q_M W m^{-2}) converted by the density of water (ρ_w in kg m^{-3}) and latent heat of fusion (L_f in J kg^{-1}).

Using the three melt algorithms, the hourly melt was computed, which was combined with the current rainfall input. New input data (for both hydrological models) consisted of P_{new} (R+M) and evaporation for each time step.

2.7. Discharge simulations

In the start of the research, we have set a spatial frame in order to validate the effect of the melt algorithms. Simulated discharge was thereby seen as indirect result of these pre-processors. We used two models to analyse effect of the pre-processors. A Sobek model was applied in the Barneveldse beek (see figure 1). WALRUS simulated Reusel, which is located in the south of the Netherlands (see figure 3).

Sobek (1-D) is an integrated surface water model. In this study, we used Sobek for rainfall-runoff simulations, for which Sobek-RR package was activated for most of the simulations. In principle, Sobek simulates runoff using three linear reservoirs; a shallow quick flow reservoir, unsaturated and saturated reservoir. These reservoirs were input according to Ernst and Krayenhoff with corresponding drainage capacities. Sobek is described in detail in the work of Prinsen (2009) and Deltaris (2014).
The case study 'Barneveldse beek' discharges water from the Veluwe towards Amersfoort. The catchment around Barneveld is part of a larger catchment South-West Veluwe (see figure 1), managed by water board 'Vallei en Eem'. The Barneveldse beek drains an area of 15816ha, of which the majority is modelled as 'unpaved' (e.g. agricultural grassland, forest). The calibration process and model properties are described in detail by Jungermann and Graaff (2013).

Figure 1: Catchment South-East Veluwe, managed by water board 'Vallei en Eem'

WALRUS is a water balance model, developed by for lowland areas. This lumped model also consists of three reservoirs; a quick flow reservoir, soil reservoir, and a surface water reservoir. Fluxes back and forth facilitate interaction between the reservoirs (see figure 2). WALRUS is introduced in the work of Brauer, et al. (2014a; 2014b). All model details and updates can be found on her site Brauer, 2015) .

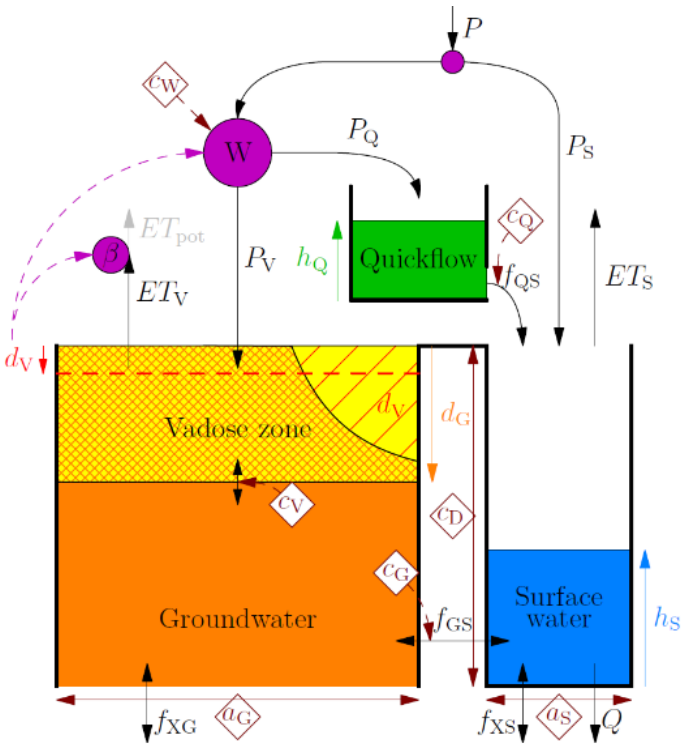

Figure 2: Schematisation of WALRUS with reservoirs, fluxes, states and parameters indicated with their abbreviations.

The Reusel catchment is a lowland catchment located in the South of the Netherlands. The catchment area is 145 km^2, managed by Water board 'De Dommel'. Similar to the Barneveldse beek, the Reusel constains mainly unpaved areas (see figure 3). (Loos 2015)

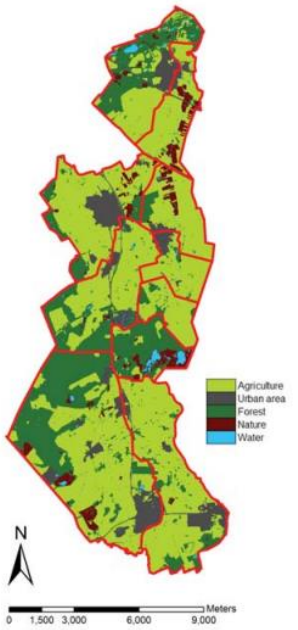

Figure 3:Land use map of the Reusel catchment (Loos 2015)

The calibrated model consisted of the following parameters (see table 2). These settings have been used for all runs.

Table 2: Model Parameters for standard discharge simulation in Reusel catchment, in the second table the catchment characteristics are presented. (Loos, 2015)

Model Parameters					**Initial conditions**
Wetness Index (mm)	Groundwater depth (mm)	Vadose Zone relaxation time (hours)	Groundwater reservoir constant (mm h^{-1})	Quick reservoir constant (mm h^{-1})	Surface water parameter: Bankfull Q (mm h^{-1})
248.6	1200	70.4	56062910	72.3	5.1

Catchment characteristics

Channel depth (mm)	Surface water area fraction (-)	Soil type	Pore size distribution parameter (-)	Air entry pressure (mm)	Soil moisture content at saturation (-)
1500	0.01	sand	4.05	121	0.395

2.8. Goodness of fit

Performance of the pre-processors was indirectly assessed by the model output of WALRUS and Sobek. Discharge observations in both study areas were used to determine the accuracy of the new simulations. A common way to assess correlation of two time series is to calculate the coefficient of determination (for linear regression this is equal to the coefficient efficient (R^2) (see equation 17).

$$R^2 = \frac{\sum_{i=1}^{n}(O_i - \bar{O})(S_i - \overline{S})}{\sqrt{\sum_{i=1}^{n}(O_i - \bar{O})^2}\ \sqrt{\sum_{i=1}^{n}(S_i - \bar{S})^2}}$$

Equation 18: Coefficient of determination R^2 for observed (O) and simulated (S) values.

In many hydrology studies, Nash-Sutcliffe Efficiency (NSE) is used even more (Krause, et al. 2005). NSE compares the (squared) variance of the observations and simulations at a reference of the mean observed values (see equation 18) (Nash and Sutcliffe, 1970). Thereby, the NSE indicates whether simulated values are better than the observed average ($0 \leq NSE \leq 1$), or worse than observed mean ($NSE < 0$).

$$\text{NSE} = 1 - \frac{\sum_{i=1}^{n}(O_i - S_i)^2}{\sum_{i=1}^{n}(O_i - \bar{O})^2}$$

Equation 19: Nash-Sutcliffe efficiency (NSE) for observed (O) and simulated (S) discharges.

These goodness of fit parameters do not assess the new simulations upon a different runoff pattern in time. Accuracy of runoff peaks is correctly measured by a NSE, even though the timing is not included (Krause, et al. 2005). Simulated discharge behaviour was analysed differently. Stream flow behaves differently due to the surface storage of snow. Runoff peaks are often delayed. If snowfall is predicted

well, timing of the peaks would be (more) similar to the observations. This change is hard to judge by a NSE, as NSE does not include a time shift in its criteria. Hence other criteria were used as well as NSE. Corresponding behaviour was measured best by the cross-correlation (CC) of discharge graphs. Without judging upon offset and scale, the dependence structure was examined in time (hourly lags^{-1} (k in equation 19)) (Salas, et al. 1980). By this means, the model error would be of less influence in the quality assessment.

$$CC_k = \frac{\sum_{t=1}^{n-k}(O_t - \bar{O}_t)(S_{t+k} - \bar{S}_{t+k})}{\sqrt{\sum_{t=1}^{n-k}(O_i - \bar{O}_t)^2 \ \sum_{t=1}^{n-k}(S_{t+k} - \bar{S}_{t+k})^2}}$$

Equation 20: Cross-correlation coefficient CC_k for observed and simulated discharge per time step (t in hours) with hourly lags (k).

3. Results

2.9. Snow occurrence in the Netherlands

A thin layer of snow covers the Dutch lowlands for several days on annual basis. In the last 10 years, an average snow cover of 11.7 cm is observed by the KNMI precipitation stations (average annual variation shown in Annex A.3). On average, Dutch snow covers melt within a week, although recently a continuous snow cover was observed for 21 days in the winter of 2011. These longer events cause a major delay in discharge peak. Long lasting snow covers built up a surface storage (over 60 cm in 2011), which may melt at once.

Hence, snow melt algorithms are developed. The algorithms are tested in snow rich winters (September to March). Figure 4 shows a selection of snow depth observations at the Bilt (data by KNMI). In the last 10 years, largest snow depth is observed during the winters of 2010, 2011 and 2012. Even more important for water management, the longest continuous snow covers (h_s>1cm) are also recorded in these periods. Hence, three time frames are selected for further analysis (see table 3).

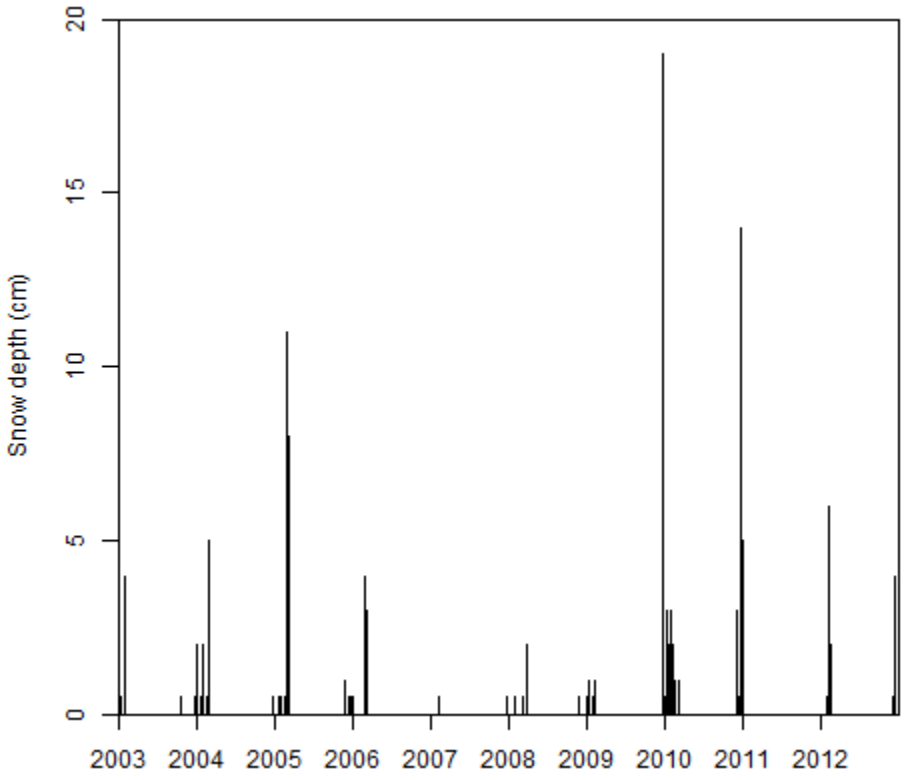

Figure 4: Snow depth (cm) observed at the Bilt in the period of 2003-2012.

Table 3: Snow event characteristics for selected winters in 2010, 2011 and 2012

Winter	Snowfall (cm)	Duration (days)	Starting day
2010	30	11	17-12-2009
2011	17	16	17-12-2010
2012	6	10	04-02-2012

In table 3, snowfall characteristics are summarized per winter. Snowfall is thereby defined as the positive change in snow depth (measured daily), since other observations are not available. Duration is also counted in days, for which a continuous snow cover was observed.

2.10. Analysis KNMI snow observations

KNMI observes snow depth on daily basis at 325 locations. Spatial variability is investigated by an interpolated (kriging) map of this data. A semi-variogram is constructed based on a long-term average (for non-zero days) snow depth at these 325 point observations (see Annex A.4). Subsequently, a model is fitted to the semi-variogram. The best fit seems to be an exponential model (least sum of squares). The variogram parameters are given in table 4. The nugget emphasises the amount of snow that cannot be explained by spatial variation, i.e. the uncertainty at point scale. The sill is a measure for the variance at independent locations, while the range indicates the spatial scale up to which observations depend on each other. The range is remarkable, since this distance is larger than the distance of individual measurement points. This may indicate the scale of variation in snow cover in the lowlands.

Table 4: Variogram model details for the long term average annual snowfall in the Netherlands (1957-2014)

Model Variogram	Nugget (cm)	Sill (cm)	Range (m)
Exponential	3.6	20.4	196082

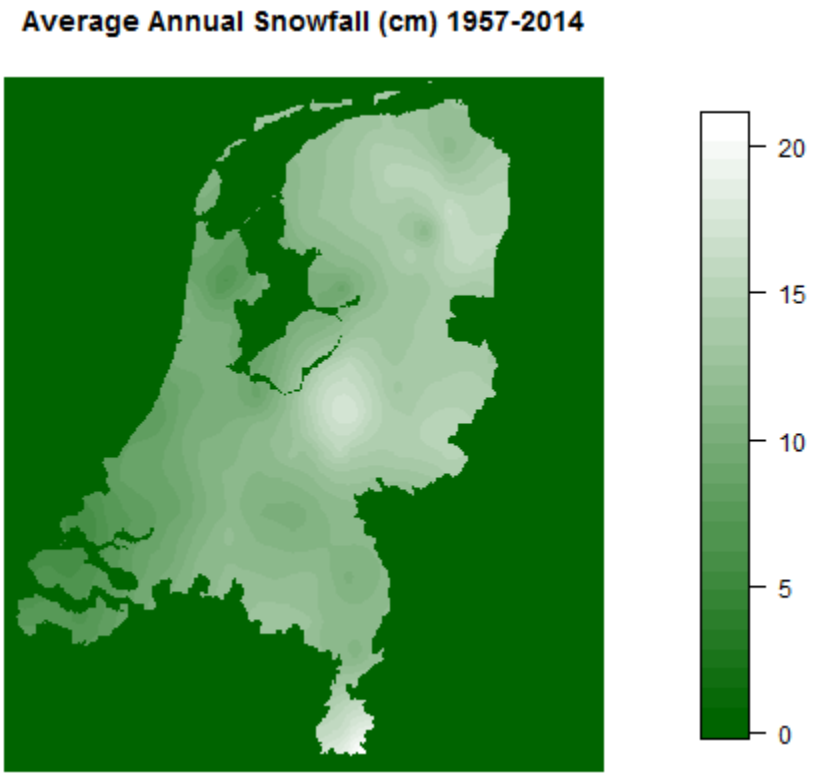

Figure 5: Average annual snowfall (cm) in the Netherlands, recorded since 1957-2014.

The long term average of the snow depth observations resulted in an interpolation snow depth map covering 1957-2014 (see figure 5), as the KNMI has been measuring snow depth since 1 January 1957. The long-term interpolation does not differ much from the last 10 years (see Annex A.5). In both time frames, the average snowfall spatial variation ranges from 6.4 to 22.7 cm in the Netherlands. Observations show a wider spectrum of spatial differences (see table 5). The interpolation seems to conduct these differences.

Table 5: Summary of minima and maxima of both the interpolated and observed snow depth data

	Minimum of dataset (cm)	Mean of dataset (cm)	Maximum of dataset (cm)
Exponential model	6.4	12.9	22.7
Observations	2.5	12.4	28.0

The interpolated snow depth map shows the average snowfall in the Netherlands. It illustrates a topographic effect, causing more snow in the Veluwe and in Southern Limburg.

2.11. Conversion of snow depth to SWE

The snow depth observations are used as validation for the SWE simulation in the surface reservoir. In this paragraph, the uncertainty of the conversion from snow depth data to SWE is explained via examples based on literature and some measurements.

The first theoretic example uses a validation set of Sturm, et al. (2010), which indicated an average snow density (ρ_s) of 0.279 g cm^{-3} for maritime climates. These climatological zones are defined on snowpack characteristics (for the exact locations see A.6). This value is used to convert the recorded snow depth of the measurement stations. The shaded area in figure 6 includes the range of uncertainty for the mean of 10344 measurements. The given standard deviation (0.098 g cm^{-3}) is used to indicate the 67% of possible snow density values.

Using the time series approach of the two papers of Sturm et al. (1998; 2010), the range of snow densities is 0.257-0.264 g cm^{-3}. The range is computed by the empirical equations for a maritime climate together with time series (hourly values are averaged to give an overview of the country). The outcome is slightly lower than the mean of the observed densities in their database.

During the research period (Sept-Jan 2014), we have observed 2 days of snow. Some measurements were carried out during the snow events. They indicate a range of 0.22-0.43 g cm^{-3} for 27th and 28th of December 2014 (detailed overview is found in Table A.7.1 and A.7.2). Simultaneously, two other measurements were carried out that indicated a snow density of 0.17-0.18 gcm^{-3} on December 27th. Summarizing these values, a wide range should be adopted in the SWE validation set. Little is known about snow density in the Netherlands and both the literature range and the observations differ to a large extent. In figure 6, a summary is given for the calculated and measured snow densities in the Netherlands. This figure is gives the SWE using snow depth data in the winter of 2011 (17th of December 2010 till 5th of January 2011).

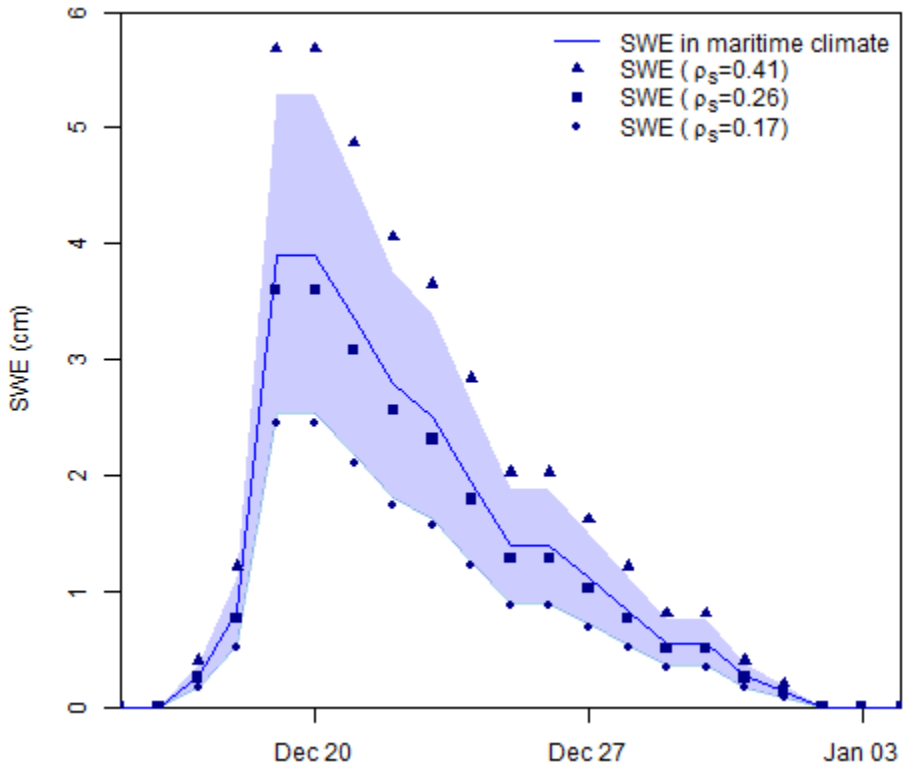

Figure 6: Example for winter of 2011 with snow depth measurement converted to SWE (cm). Conversion is done by average ρ_s for a maritime climate (blue with shaded area), in addition the average of rare ρ_s measurements used for the pointed SWE series.

2.12. Snowfall-rainfall partitioning

Three approaches have been selected from literature to separate precipitation into rain and snow. This resulted in one static temperature threshold, and two dynamic methods in which mixed precipitation is possible: the PQ model and the VIC model. See Section 2.2 for details. Hourly precipitation records at the Bilt are used as input for these models.

In figure 7, the accumulated snowfall, converted to snow water equivalent (SWE in cm) is shown for the three winters. The conversion from snow depth measurements to SWE is done using equation 20. The assumption is that any positive change in snow depth from one day to the next is related to snowfall. The grey range indicates the uncertainty in snow density. A density range corresponding to fresh snow is selected. These density rates vary among studies and many different values are reported for different weather circumstances. However, a commonly used range is between 100 and 200 g cm^{-3} (Meløysund, et al. 2007). The thick line gives the average of this range. Uncertainties and sensitivity are discussed previously (section 2.11).

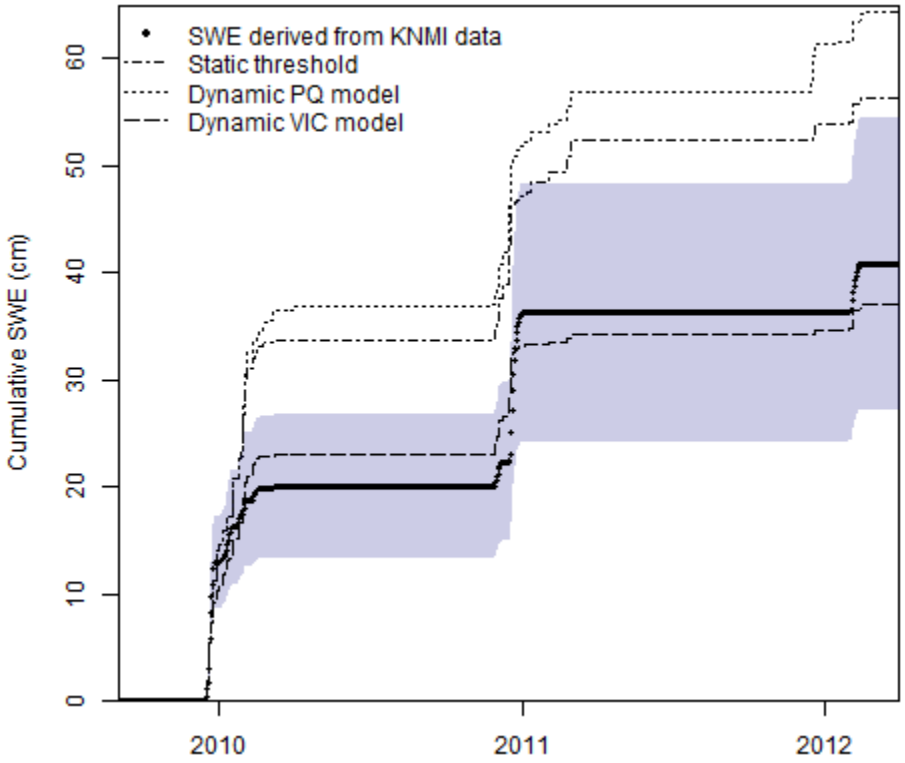

Figure 7: Cumulative SWE time series is plotted for three different models (static threshold, dynamic Pipes &Quick (PQ) and dynamic VIC model). These results are shown together with the observations at the Bilt (thick black line with shaded area). The shaded area indicates the range of possible snowfall densities.

The VIC model seems to simulate cumulative snowfall well, if these results are compared to the range of SWE in the Bilt. For all winters, the VIC model underestimated the SWE with 4.4cm, which is relatively little compared to the overestimation of 23.6cm and 15.5cm by the dynamic PQ and linear model. Hence, the VIC model is used to compute snowfall input for the melt algorithms.

2.13. Melt-algorithm comparison

The total snowfall is thus determined using the VIC model. Snowfall is an input for the surface reservoir, which is depleted due to modelled snowmelt. The three different snow algorithms resulted in different SWE melt pattern, which are shown in figure 8.

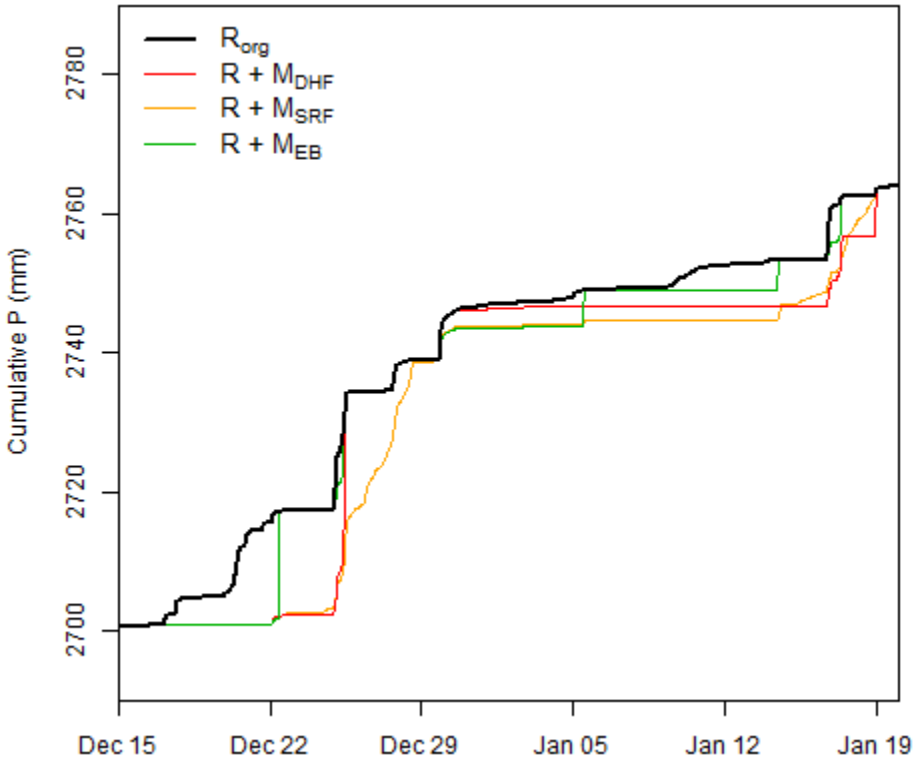

Figure 8: A close-up from a cumulative precipitation time-series plot shows the predicted melt in the winter of 2009-2010 (the entire series starts in January 2007). The thick black line indicates observed rainfall (interpolated from 7 weather stations). The coloured lines represent the three melt algorithms.

The complete cumulative precipitation series starts at the warming-up period of Sobek (January 2007), but only a part is shown to visualize melt in figure 3. The compilation of rain and melt is visible for the three models, as a reference the observed rainfall is also shown (thick black line). The observed rainfall series is a result of 7 weather stations recordings that are interpolated in Sobek. The weather stations are the Bilt, Deelen, Barneveld, Heelsum, Lunteren, Wageningen and Woudenberg.

The surface reservoirs start and end empty (all lines are converged), and they start to differentiate at different moments in time. Similar findings are found for the two other winters (results in Annex: A.8+ A.9).

Modelled snow storage (SWE) is shown in the figure 9 for the same period. The figure gives a detailed image of the SWE fluctuations in time. The snow event lasted from the 17th of December to the 18th of January in 2010. The coloured lines indicate the three algorithms. Change in SWE represents the filling (snowfall) and depletion (melt) of their surface reservoirs. Remarkable is the difference in timing of snowmelt. Moreover, the large peak of the observed SWE around 20th December does not correspond entirely to the simulated melt. The first winter is overestimated by VIC (see figure 7), so in theory more snow would be present in the snow reservoir than observed. Nevertheless, KNMI observations indicate

more SWE than modelled. The shaded area around the observations indicates the range of possible snow densities. The range differs from the earlier used snow densities: snow depth measurements correspond to 'settled' or 'compacted' snow, in contrast to snowfall that was discussed in section 3.2. Therefore a range of snowpack densities in a maritime climate is used to compare the modelled SWE to the snow depth measurements (181 to 377gcm^{-3} based on the work of Sturm, et al. (2010)). Details about this range are explained previously in paragraph 2.11. However, the densities used in Sturm, et al. (2010) are derived from generally much thicker snowpacks than occur in the Netherlands. The uncertainty in the snow density may well be larger than indicated in figure 9.

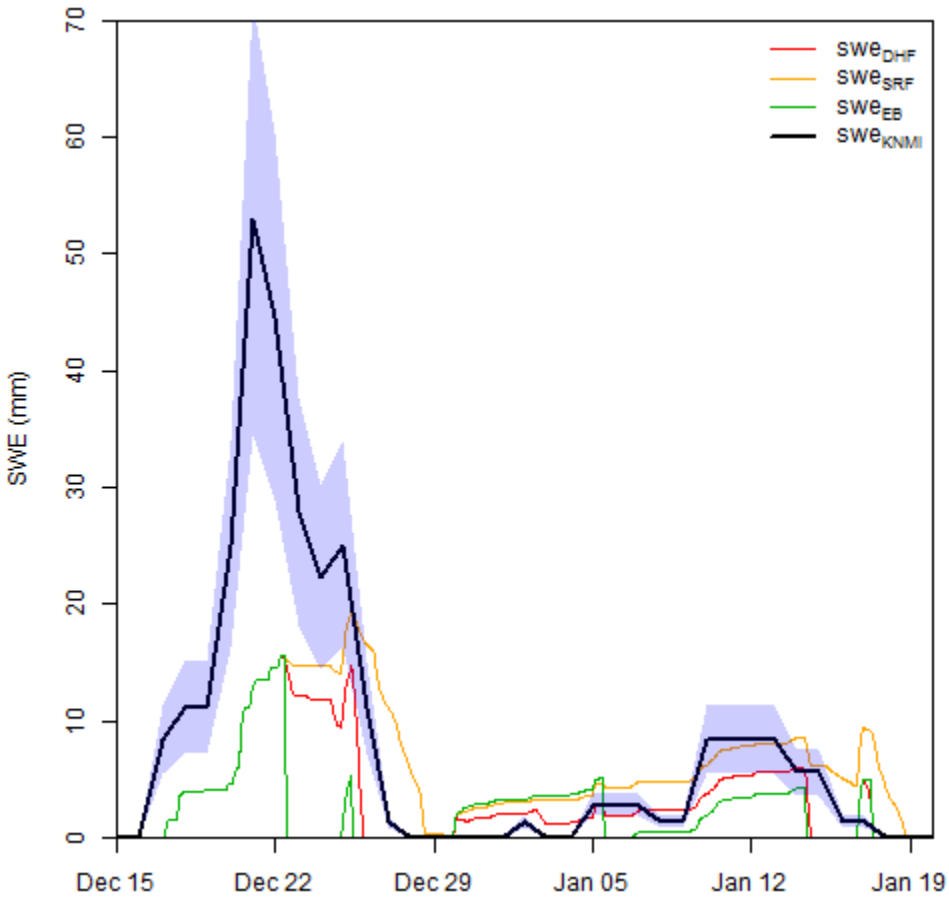

Figure 9: SWE time series of observed records (black line with shaded area), hourly-degree day model (swe_{DHF} in red), shortwave radiation model (swe_{SRF} in yellow) and the energy balance (swe_{EB} in green). Results for the winter in 2009-2010 are shown. Results for other winters can be found in Annex (A.10+ A.11).

2.14. Model results

3.6.1. Barneveldse beek (Sobek-RR)

Discharge simulations using Sobek-RR are forced using precipitation series at seven KNMI stations, of which one is De Bilt. The results described in previous sections thus partly overlap with the graphs that are shown here. As a result of the melt algorithms, discharge series differ from the original time series (see figure 10). A detailed explanation is given for the first winter, followed by a short overview of the results for 2011 and 2012.

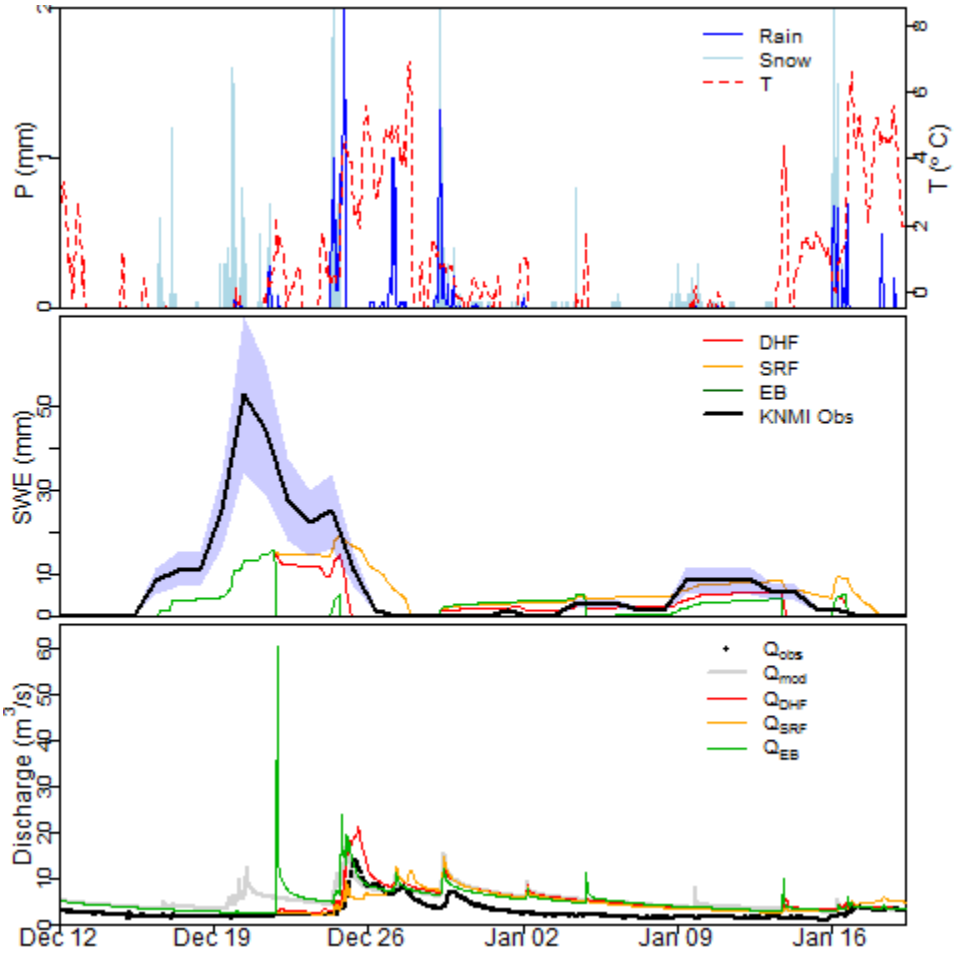

Figure 10: Discharge simulations for Barneveldse beek using Sobek. In the first plot the separated precipitation and temperature are seen. Air temperatures above -0.5 ℃ are also shown. The second plot shows the simulated SWE and its decrease, in addition the derived SWE from KNMI observations are shown with the uncertainty range for snow density (shaded area). In the last graph, the simulated discharge is shown for all models (incl. original in grey) together with the observed discharge. Results for other winters are found in A.12+A.13 in Annex.

The first graph shows the precipitation separation together with the average temperature per time step. In the figure, the second Y-axis for temperature is set to the lower boundary for rainfall (−0.5 ℃), so that modelled rain (and snow mixture) is easily compared. Air temperature (T_a) is the main driver for both the precipitation separation and the temperature-index algorithms (DHF and SRF). The energy balance algorithm also contains components that are directly affected by T_a (Q_H, Q_R and Ln). Nevertheless, the

major melt peak around 22nd of December is also caused by other fluxes. An overview of these fluxes can be seen in figure 11.

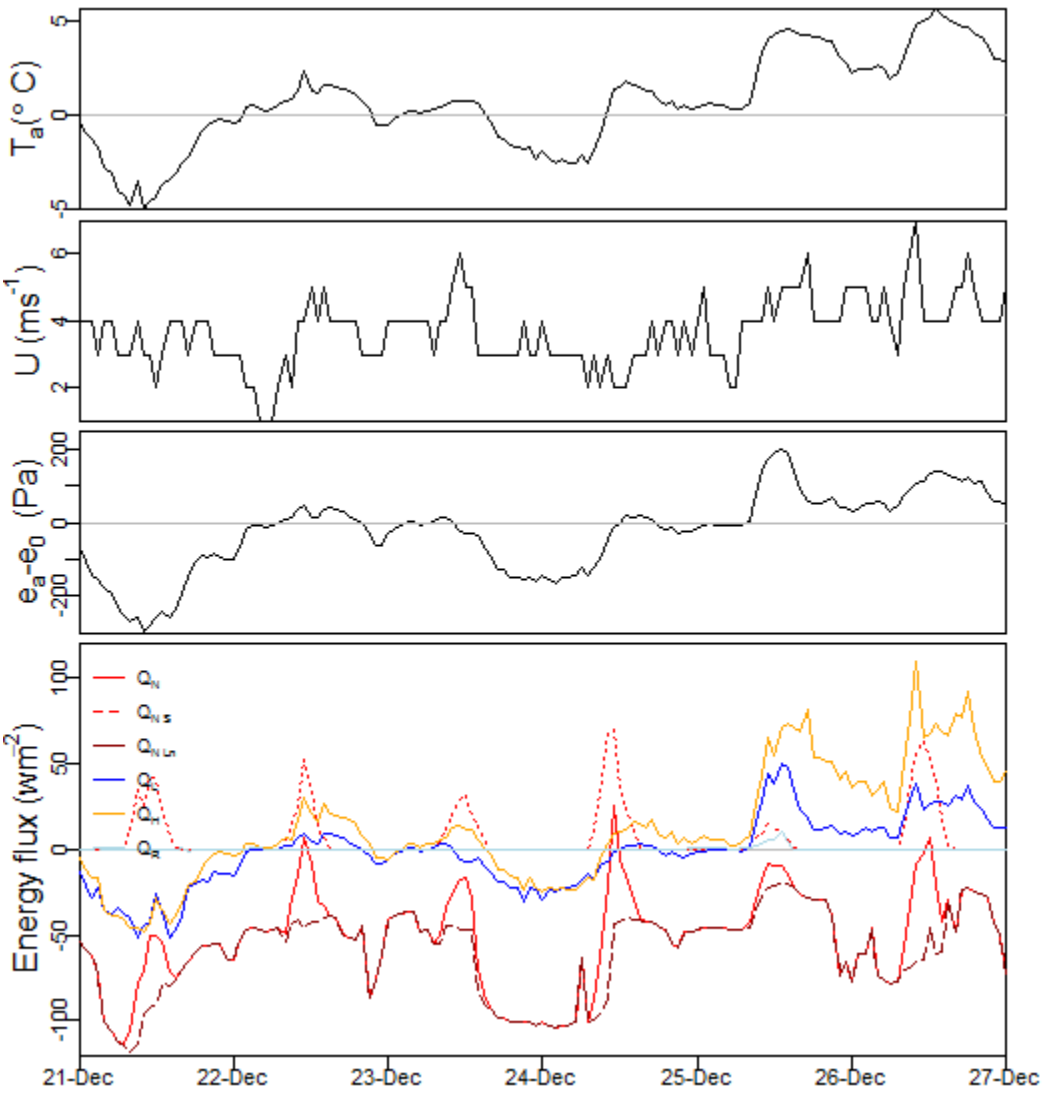

Figure 11: Input variables and fluxes of the energy balance. In the first graph hourly air temperature (℃) is shown. The second plot shows average wind speed (m s^{-1}). The vapour pressure balance (Pa) is shown in the third plot. Finally, all fluxes of the energy balance (W m^{-2}) are shown in the last plot.

In the lowest graph in figure 11, all fluxes of the energy balance are shown for this particular melt event. In the three first graphs, the climate variables are displayed. These input variables are the main drivers for the energy fluxes. First, T_a shows an increase at 22 December 2009 and peaks just above freezing point. Wind speed and vapour gradient peak at the same day. These three components drive the turbulent fluxes (see equations 11+13). In addition, global radiation increases (observations are not shown), which is directly reflected in the shortwave component of the net radiation flux (dotted red line). Since a constant value is assumed for the albedo, a fixed proportion of the global radiation is included in the energy balance. The available energy for melt is in this case an accumulation of the net radiation flux together with the increase of the two turbulent fluxes (yellow and blue line in lowest graph). The melt energy is

reviewed in the sharp SWE decrease (depletion of surface reservoir) and the peak discharge visible in figure 9 and 10.

The winters of 2011 and 2012 show similar features to the first elaborated example (see A.12 and A.13 in Annex). In the winter of 2011, a gradual melt pattern is simulated by the two temperature-index algorithms. The energy balance algorithm (once again) simulates a sudden depletion of the snow storage reservoir, caused by a sharp increase of temperature. Even though the degree-hour algorithm depends on air temperature, this algorithm seems to be less sensitive to sudden temperature changes than the energy balance. SWE simulation of DHF shows a gradual decline compared to the steep decrease of the EB algorithm.
Snowmelt for the last winter (2012) is simulated fairly similar by all melt algorithms. The surface reservoirs depleted in a relatively short time spend, but compared to the other selected winters, a relatively shallow snowpack was present.

To assess whether the snow algorithms improved the modelling result, the goodness of fit is analysed by comparing discharge simulations to the observed discharge in the Barneveldse Beek. For the majority of the simulations, a negative Nash-Sutcliffe efficiency (NSE) is calculated. When the melt algorithms are included, NSE are less negative compared to the original Sobek-RR simulation. Less negative NSE still imply that results simulate less good than the observed mean. Regardless the negative NSE, melt algorithms tend to improve the discharge simulation visually. Note that the Sobek-RR model was not re-calibrated for this study. The original calibration was performed on a different (multi-year) period with the objective of simulating peak flows. Moreover, the RR model simulates discharge on plot level in a distributed manner throughout the catchment. These flows were summed to obtain the catchment total, but routing is not applied. These simulations are compared to the observations, which are measured at the outlet of the catchment. In Sobek, a hydraulic model (1D channel flow model) simulates water transport through a channel network. In these simulations, discharge is slightly delayed and peaks are flattened out compared to the RR model simulations. This flattened peak affects the NSE, since this method is sensitive to overestimated peak flows (Krause, et al. 2005). Hence, an extra run is performed that includes the 1D model (see figure 12).

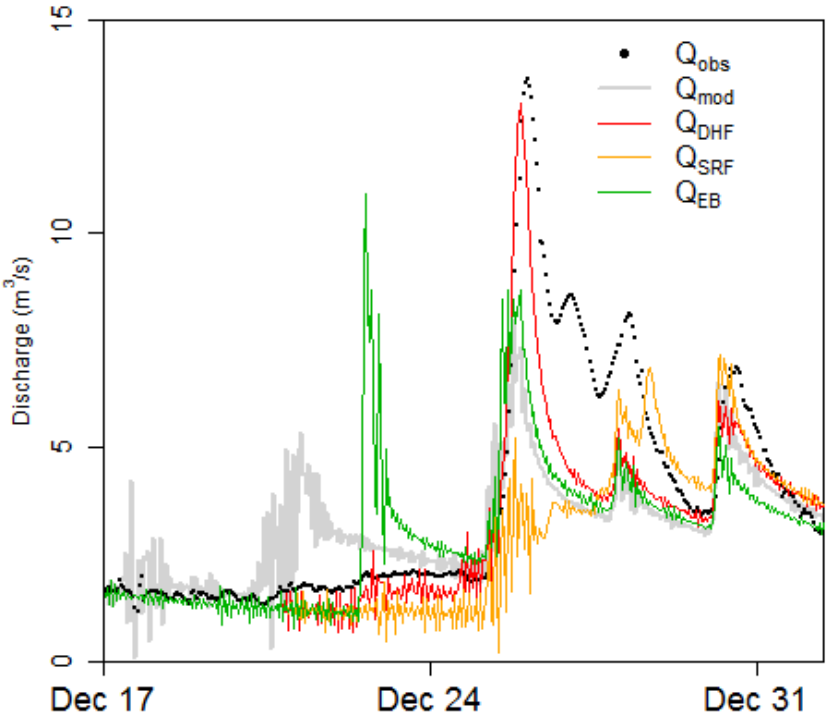

Figure 12: Discharge simulations for Barneveldse beek using Sobek RR and 1D model. The original discharge simulation is shown in grey. The coloured lines indicate the three models and the points show the observed records.

In this extra run, some differences are visible. First of all, the maximum peaks differ to a large extent. The overestimation of the EB algorithm is still present (peak at December 22), but its overestimation is much less compared to the RR model simulation. Another difference is the predicted melt peak of the DHF melt algorithm that corresponds well, although the simulated recession curve differs from the observed series. A remarkable change is the instability of the modelled discharge series. These small fluctuations are probably caused by weir close to the measuring location.
All these differences to the original Sobek-RR output, have major influence on the Goodness of Fit parameters, which is reviewed in the first column of table 6.

Since negative NSE values indicate only that the simulations are worse than the observed mean, we have also used the R^2 to quantify the change in simulation performance using the snowmelt algorithm. An example of a melt peak is shown in figure 13, the SRF algorithm performed well on this event (see table 6).
The corresponding behaviour is analysed by the cross-correlation. Cross-correlations compare two time series without considering scale and offset. In this way, the model-error would be of less influence. The comparison is based on the correlation between the observed and simulated time series for a range of time lags (in hours, up to 24h). High correlations are achieved for simulations that follow the observations simultaneously. In table 6, average cross-correlation is given for the time series. To show the difference for one winter, an example is shown in figure 14. An overview is given for all model results in table 6.

Table 6: Goodness of Fit for Sobek (RR +1D and RR) model for all winters

	RR + 1D model Winter of 2010	RR model Winter of 2010	RR model Winter of 2011	RR model Winter of 2012

GoF	NSE	R^2	CC	NSE	R^2	CC	NSE	R^2	CC	NSE	R^2	CC
Q_{Org}	0.39	0.49	0.55	−1.14	0.44	0.62	−0.77	0.16	0.28	−1.02	0	0.10
Q_{DHF}	**0.73**	**0.80**	**0.67**	−0.79	**0.78**	**0.74**	0.13	0.48	0.55	−0.84	0.06	0.22
Q_{SRF}	0.28	0.41	0.57	−0.51	0.44	0.63	**0.42**	**0.67**	**0.67**	−0.83	0.06	0.22
Q_{EB}	0.39	0.45	0.54	−1.97	0.24	0.49	−0.52	0.21	0.35	−0.83	0.06	0.22

In the winter of 2011, a clear improvement is made by the melt algorithms. The NSE turns positive and R^2 is also improved. The CC histogram for this event shows a higher average correlation with the observed discharge series.

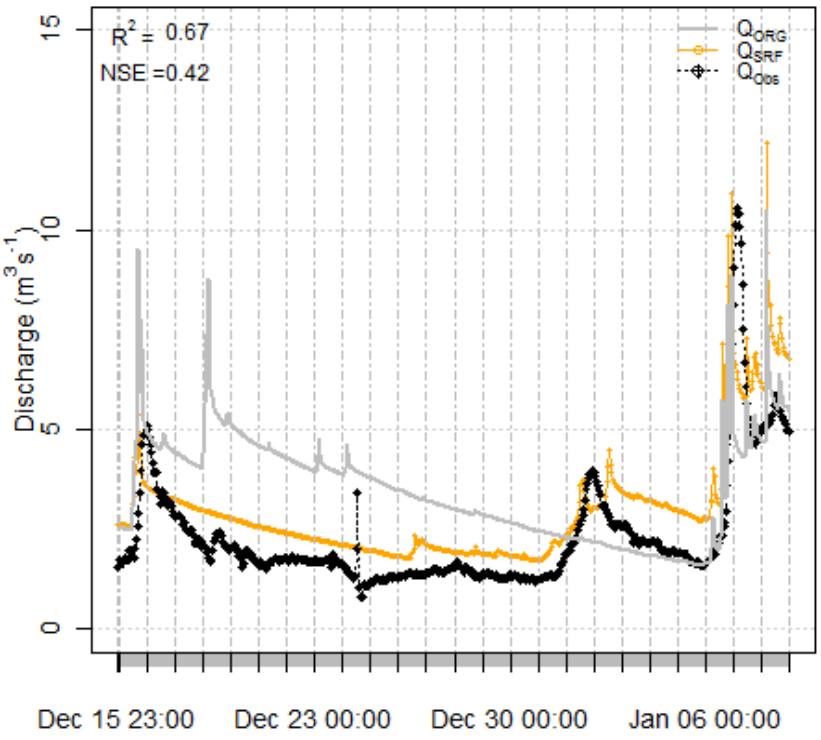

Figure 13: Goodness of fit for Q_{SRF} in the winter of 2011. R^2 indicates a performance of 0.67, NSE is 0.42.

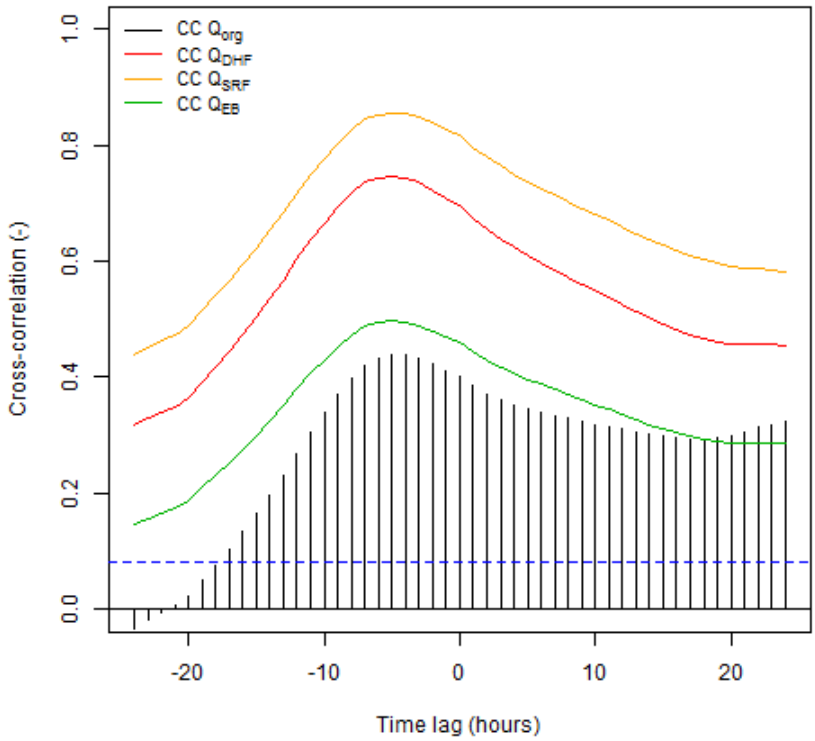

Figure 14: Cross-Correlation plot for the observed and simulated discharge time-series in the winter of 2011. Correlation is shown for 24h, in black (bars) the original discharge series is indicated. Red, yellow and green indicate the melt algorithms (DHF, SRF, EB consequently).

In general, the melt algorithms change the current discharge series and they seem to improve the series in many cases. The two temperature-index algorithms achieve higher correlations, but there is not a clear difference between the two. Hence, a second case-study is performed using the WALRUS model in a different catchment.

3.6.2. Reusel (WALRUS)

Discharge simulations in the Reusel are analysed similarly to the simulations of the Barneveldse beek. In addition, a detailed view is given for the standard run and first winter of 2009-2010.

The model has already been calibrated on hydrological year 1998 by Loos (2015). These settings result in the following simulations for the 'standard' winter periods in the Reusel catchment (see table 7).
The simulated fluxes indicate the interactions between the reservoirs. In the last columns of table 7, begin and end values are shown for the states in the reservoirs. In figure 3, a schematisation of WALRUS is shown (with abbreviations).

Table 7: WALRUS simulations for a standard runs in the three winters, model is calibrated by Loos (2015).

WINTERS		Simulations (all measured in mm h^{-1})			Fluxes (all measured in mm h^{-1})				Difference in states (all measured in mm)			
Start Date	**End Date**	Et_{pot}	Q_{Obs}	Balance	f_{XG}	f_{XS}	f_{GS}	f_{QS}	d_V	d_G	d_{hQ}	d_{hS}
12 Dec 2009	**20 Jan 2010**	9	44	23	0	0	1.6	41.5	24.6	99.7	−1.1	−0.1
15 Dec 2010	**8 Jan 2011**	5	30	24	0	0	1	28.8	21.9	68.8	2.1	0.3
29 Jan 2012	**01 Mar 2012**	16	20	-3	0	0	1.1	17.9	0.8	6	−3.4	−0.5

These settings give a good agreement for hydrological years 2009-2012: NSE ranges from 0.7-0.83. However, the winter simulations' predict less accurate, see the example (the winter of 2009-2010) in figure 15 (original output format of WALRUS).

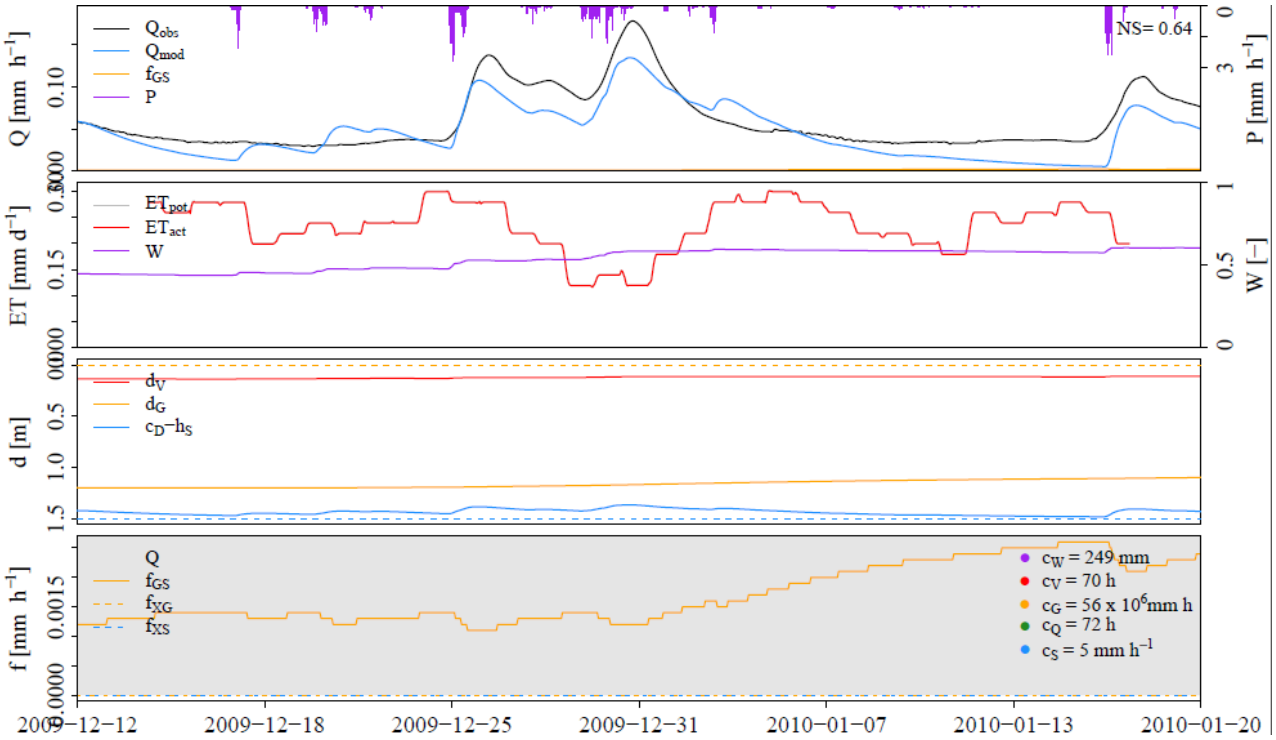

Figure 15: WALRUS output for winter 2009-2010 in Reusel catchment (original WALRUS format).

The melt algorithms are implemented in WALRUS, and their influence is shown in figure 16, which is built up similar to the Sobek figures. Precipitation (rain and snow) are shown in the upper graph, SWE is plotted in the middle graph and the lowest graph contains discharge simulations together with the observed values (note that the unit differs from the figure 10, in this case specific discharge is shown).

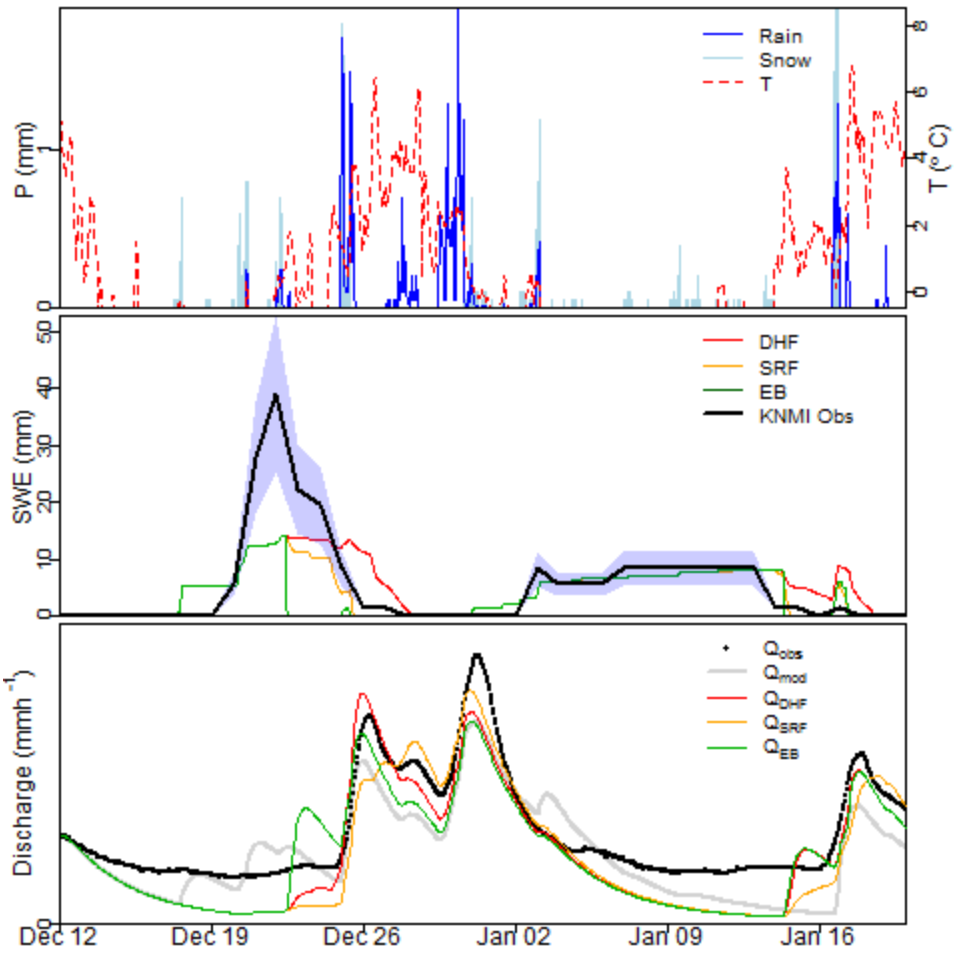

Figure 16: Discharge simulation of the Reusel catchment using WALRUS. In the first plot the separated precipitation are seen. Air temperatures above −0.5℃ are also shown. The second plot shows the simulated SWE and its decrease, in addition the recorded KNMI values (with an uncertainty range: shaded area) are displayed. In the last plot the simulated discharge is shown for all models (incl. original) together with the observations.

In the same period (winter of 2009-2010), less rain fell at the weather station in Eindhoven compared to the precipitation records at the Veluwe (Barneveldse beek). This is also seen in the middle (SWE) plot, since both the simulated and the recorded SWE show lower values than simulated in Barneveld. However, the underestimation for SWE prediction seems to be consistent with the case of the Barneveldse beek. The last graph shows the effect of the melt algorithms on discharge. In general, standard discharge series have a good agreement with the observations, although the observed base flow is generally higher than modelled. The melt algorithms produce increased discharge peaks, but the timing of the peaks does not correspond completely with that of Q_{obs}.

In general, the WALRUS simulations agree better with the observations than the Sobek model does. For the hydrological years, the NSE ranges from 0.70-0.83. Winter simulations performed less good (see table 8), but the melt algorithms changed these efficiencies positively. The correlation coefficient (R^2) shows stable or an increased correlation with the use of melt algorithms.

Table 8: Goodness of Fit for WALRUS in Reusel for all winters

	Winter of 2010			Winter of 2011			Winter of 2012		
GoF	NSE	R^2	CC	NSE	R^2	CC	NSE	R^2	CC
Q_{ORG}	0.64	0.77	0.80	−0.72	0.07	0.16	−0.1	0.77	0.83
Q_{DHF}	0.70	0.90	0.88	0.24	0.68	0.70	−0.2	0.78	0.84
Q_{SRF}	**0.67**	**0.91**	**0.90**	−0.33	**0.83**	**0.75**	−0.2	**0.80**	**0.85**
Q_{EB}	0.63	0.81	0.83	−0.07	0.09	0.22	−0.2	0.77	0.84

Cross-correlation indicates a consistently better agreement, although the improvement itself differs for the tested winters. An example of an increased CC is shown for the winter of 2011 in figure 17. The DHF algorithm shows a consistent improvement (over all time lags), but for the majority the SRF algorithm performs best. Only referring back in time (negative lags), the correlation for the simulation is less than for the DHF algorithm.

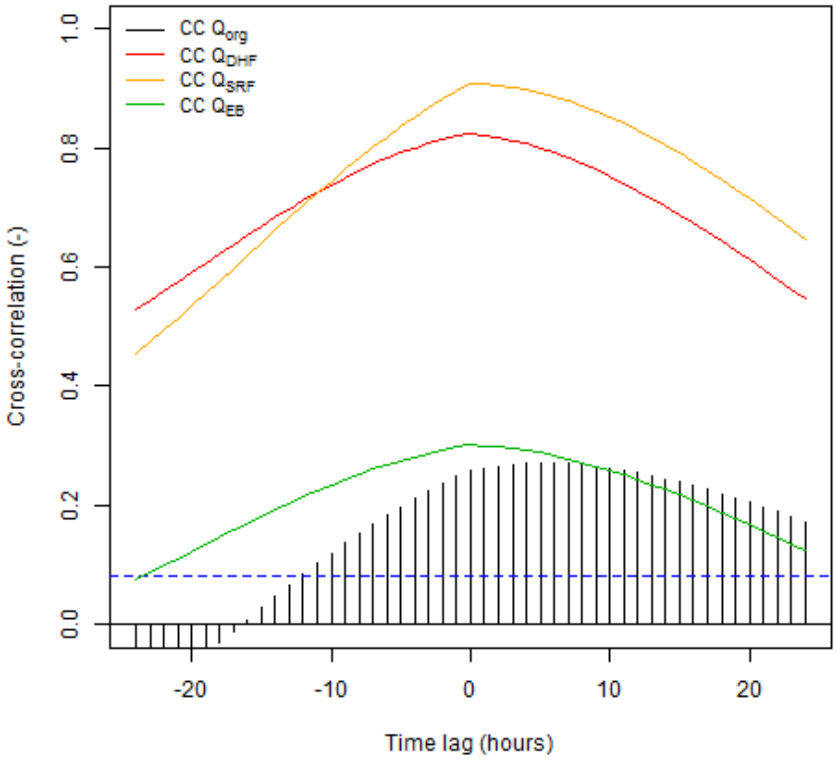

Figure 17: Cross-Correlation plot for the observed and simulated discharge time-series in the winter of 2011 (modelled by WALRUS). Correlation is shown for 24h, in black (bars) the original discharge series is indicated. Red, yellow and green indicate the melt algorithm (DHF, SRF, EB consequently).

2.15. Sensitivity analysis

3.7.1. Solid/liquid precipitation

Separation of rain and snow can be done in multiple ways, as discussed previously. We have applied a gradual transition (section 2.2). Boundaries to distinguish either solid or liquid precipitation have been set

based on similar literature studies. Observations show a wide band of temperature ranges for increasing snow depths (Kienzle, 2008; Loth et al., 1993). As snow depth is measured daily by KNMI, only daily (maximum/minimum) air temperatures can be related to find reliable boundaries.
The maximum air temperature indicates a threshold, at which snow still fell. Related studies report a wide range with a maximum of 14℃ (Kienzle, et al 2008). Dutch observations indicate a range from −7℃ up to 10.6℃ (based on KNMI data). A complete picture of the temperature distribution (T_{mean}, T_{min}, T_{max}) is seen for days with snowfall in figure 18. Even though, daily records do not follow a perfect Gaussian distribution, the daily mean and standard deviation values have been used to capture the majority of maximum daily temperature range. By the dotted grey lines, these boundaries are indicated in figure 18.

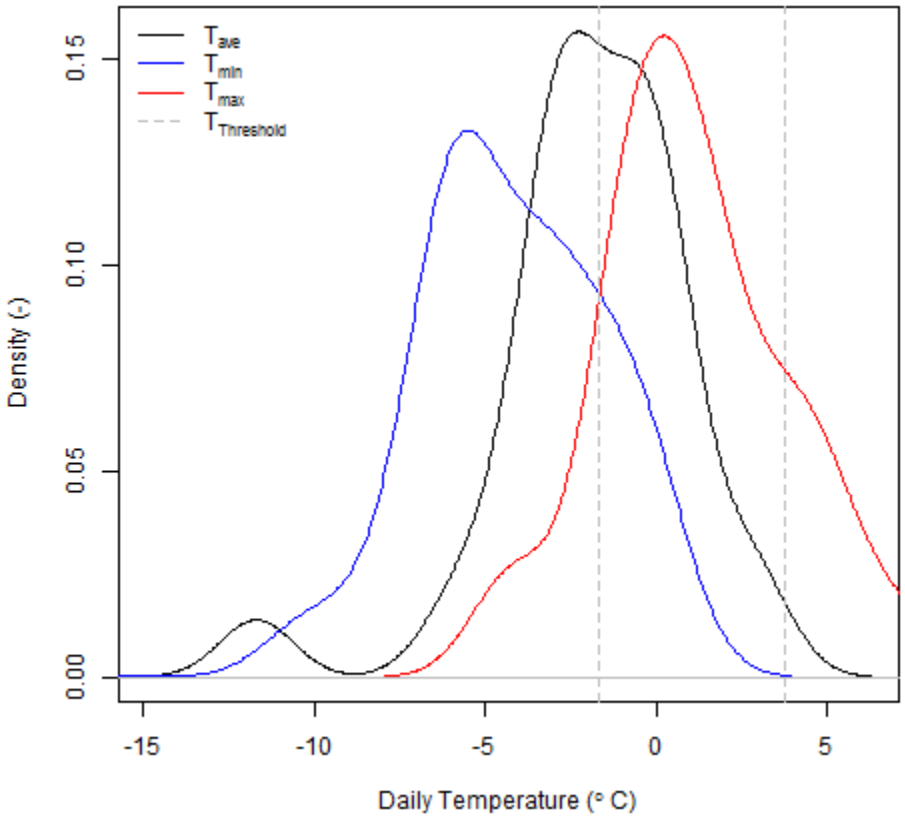

Figure 18: Density plot of the daily maximum, average and minimum temperatures plot together with the new temperature thresholds ($T_{Threshold}$ in grey)

As a result of these new boundaries (T_{snow} = 3.8℃ and T_{rain} =−1.7℃), the percentage of rain and snow differs in the simulations. This affects not only the snow parameters, but the resulting changed energy fluxes may also alter runoff simulations, as stated previously by (Loth et al., 1993). He argues that snow cover models are strongly sensitive to these parameters.
In fact, when recalculating the modelled SWE with new threshold values, only the SRF model responds to the changed temperature boundaries (see figure 19). The dotted lines indicate the new runs based on precipitation series in Eindhoven. The energy balance seems to be less affected than initiated by literature.

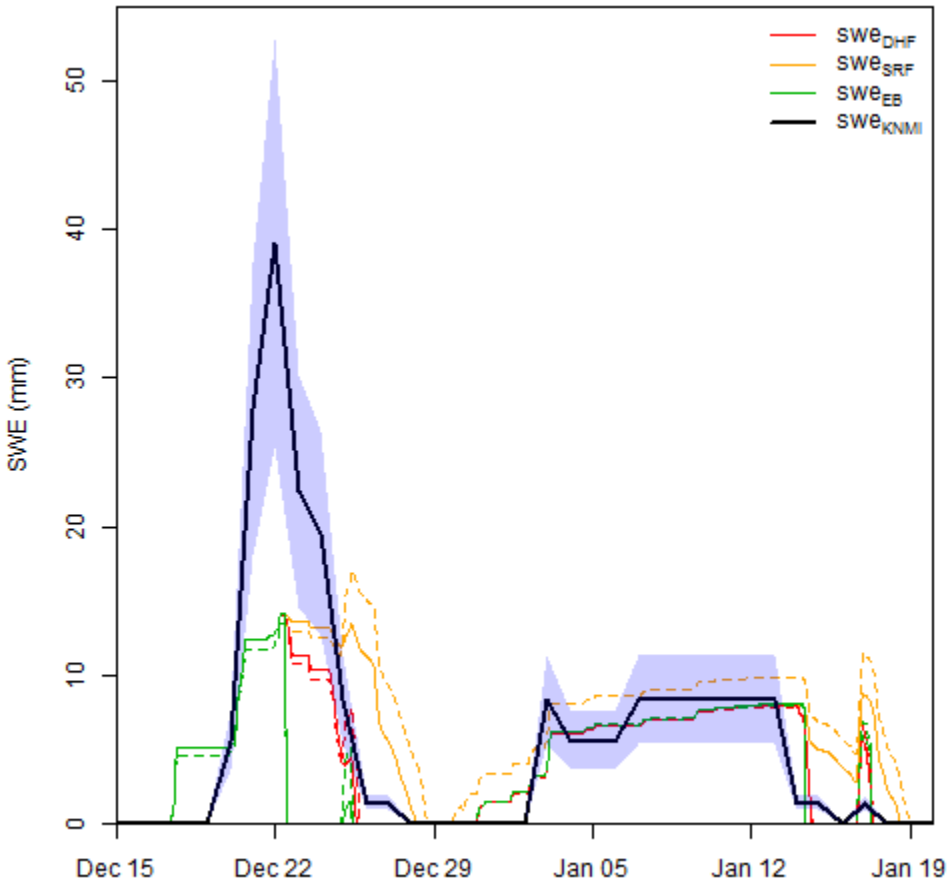

Figure 19: Modelled SWE for the precipitation data in Eindhoven. The dotted lines indicate the difference with new (wider) temperature thresholds for the snow and rain separation.

Discharge simulations (results not shown) show some difference visually, but the results are assessed best by the goodness of fit parameters (see table 9). The DHF module increases most (proportionally) in the parameters. The energy balance benefits also from the wider temperature range. SRF is affected negatively, as shown by the overestimation in the surface reservoir in figure 19.

Table 9: Goodness of fit parameters for the sensitivity case of winter 2010, results are only applicable to the melt algorithms. Results are modelled using WALRUS in the Reusel.

	Original case Winter of 2010			Sensitivity case Winter of 2010		
GoF	NSE	R^2	CC	dNSE (%)	dR^2 (%)	dCC (%)
$\mathbf{Q_{DHF}}$	0.70	0.90	0.88	4	1	0
$\mathbf{Q_{SRF}}$	0.67	0.91	0.90	−14	−7	−2
$\mathbf{Q_{EB}}$	0.63	0.81	0.83	3	1	1

3.7.2. Energy balance

An accurate prediction of melt is desired. Therefore an attempt has been done to combine all energy fluxes in a snowpack energy balance. If all fluxes are simulated correctly, an energy balance can predict melt in great precision (Hock, 2003; 1999). However, many climate variables are required to simulate the incoming and outgoing fluxes. In our case, the automatic weather stations provided the majority of the data. In the time series of the observed cloud cover some gaps were found (in total 41 observations). These gaps have been filled by the assumption that during a precipitation event the sky was fully covered (m_c=1). In absence of precipitation, a clear sky was assumed (m_c=0).
Filling these gaps raised the question, if these values would affected the energy balance outcomes. Hence, this assumption and two others: the constant snow surface temperature and the local global radiation, are researched in order to verify the sensitivity of the implemented energy balance (for results see table 10). The total available energy for melt is thus analysed for three sensitivity cases (from December 21st to 27th 2009). During these 7 days, a large melt event is simulated that is not supported by the observations. Since the total amount of melt energy is questioned, the sum of the individual fluxes in the energy balance is shown in table 10. The changed fluxes are given in percentages.

The cloud cover sensitivity is investigated by replacing either a clear sky or a covered sky for a specific time period. The effect is seen in the change of the longwave radiation (in percentages reviewed in table 10). Moreover, a clear difference is seen in the energy available for melt. This is over 60% higher the period for clear sky compared to the standard. In practice, this percentage implies that less energy is available for melt (60% increase of a negative energy for melt), clouds thus enhance the melting of the snowpack. So far, the Dutch data and case is corresponding to previously researched phenomena (Hock, 1999; Marks, et al. 1998).

The constant snow surface is assumed to be zero in the equations of the longwave radiation, latent heat, sensible heat and sensible heat flux of rain. For these equations, the assumed temperature is lowered to −1 ℃. Consequently, the maximum vapour pressure is also adjusted to 563Pa (instead of 610Pa). This is the maximum vapour pressure of a snowpack surface at −1 ℃ (equation by KNMI 2000:67).
As a result, the net radiation flux shows a minor change. This change is due to the change for longwave radiation, which reacts upon an altered temperature gradient. The effect for the latent heat flux is enormous (Q_L becomes +965 Wm^{-2} $7d^{-1}$). This flux seems to be very sensitive to this assumption. The sensible heat flux and the sensible heat flux of rain show a positive change, but not so drastically as the increase of the latent heat flux. In total, more energy is available for melt due to the increased temperature gradient. Note that for a complete comparison with related studies Q_G should also be included.

The last topic of research is the observed global radiation. This factor seems to influence the melt rate at 22 December 2009 (see the peak discharge at December 22nd in figure 10). Hence, it is researched whether local measurements affect the melt simulation. Global radiation measured at the Deelen is taken as an alternative for the current observations. The distance to the Barneveldse beek is approximately 24 km east (as the crow flies) compared to 30 km west for the weather station at the Bilt.
The radiation component has only little influence on the melt energy. The shortwave radiation component increases, but only 1 % change is simulated in this particular period on the general snowpack balance. In total, there is a more energy available for melt in these 7 days, but the local changes seem to have minimal influences to the total balance.

Table 10: Fluxes of the energy balance (Q_N,, $Q_{N\,S}$, $Q_{N\,LN}$, Q_L, Q_H, QR and Q_M) during 21-27 December 2009 in the first column. From the second column onwards the relative change is given in percentage (as the relative change to the standard run).

	Q_N	$Q_{N\,S}$	$Q_{N\,LN}$	Q_L	Q_H	Q_R	Q_M
Standard ($Wm^{-2}7d^{-1}$)	−7587	1058	−8645	−305	1727	32	**−6133**
m_c =1	−43%	0%	−38%	0%	0%	0%	**−54%**
m_c =0	51%	0%	45%	0%	0%	0%	**63%**
T_s =-1℃	−7%	0%	−6%	−416%	85%	70%	**−54%**
G (Wm^{-2}) (Deelen)	−1%	6%	0%	0%	0%	1%	**−1%**

3.7.3. Base temperature for melt

The DHF and SRF algorithms simulate snow melt by a temperature-index melt model, forced by the observed air temperature and a base temperature. Melt will be often simulated, if average air temperatures (T_a) are positive in a certain timescale (Kustas, et al. 1994). Base temperatures do not have to be exactly zero. A variety of thresholds is defined by other studies. This variety may account for potential differences in time and space (Hock, 2003).
In this study, melt is assumed to occur if T_a exceeds 0.5℃. However, a daily decrease in snow depth (melt) is observed in a wider range of maximum daily temperatures (−5℃ to 9 in℃) than this static threshold assumes (KNMI data).

Due to data availability, only daily temperatures can be related to melt events. Maximum daily recordings may indicate the lower threshold on hourly basis, eventhough this range is largely negative (up to −5℃). Lowering thresholds results in earlier melt, less SWE and an earlier peak in runoff discharge (seen in the hydrographs in figure 20). For the DHF model, simulated melt is considerable higher in winter of 2009-2010. SRF is less sensitive to this change, as it is expected by the semi-empirical melt algorithm (Kustas, et al. 1994). Besides air temperature, shortwave radiation is also taken into account for melt.
In table 11, the change in terms of the goodness of fit parameters is shown. Specifically, the large (negative) change in NSE is remarkable, as they become more negative. It is once again indicated that the NSE method is highly sensitive to deviations peak flows.

Table 11: Goodness of fit for the changed base temperature modelled in Barneveldse beek in winter 2009-2010

	Standard case Winter of 2010			Changed base temperature Winter of 2010		
GoF	NSE	R^2	CC	dNSE (%)	dR^2 (%)	dCC (%)
Q_{DHF}	−0.79	0.78	0.74	65	−22	−9
Q_{SRF}	−0.51	0.44	0.63	92	−2	−2

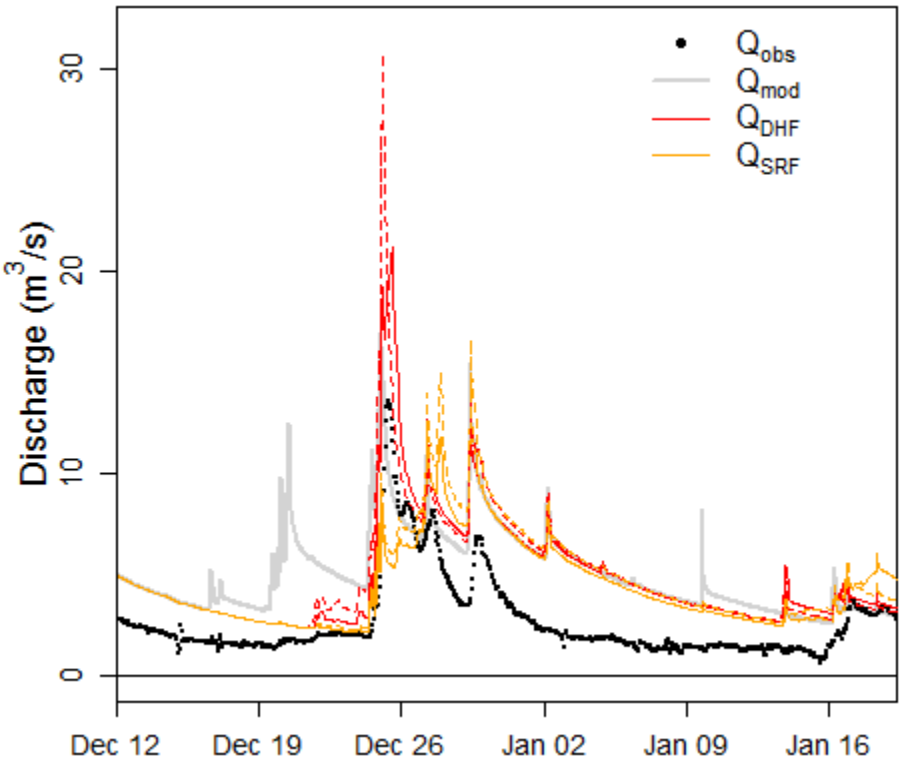

Figure 20: Simulated discharge for the Barneveldse beek using Sobek for the winter of 2009-2010. The dotted lines indicate the difference with the base temperature on 0.5℃.

4. Discussion

3.1. KNMI snow observations

Annual averaged KNMI snow depth observations show little spatial variability, as the range of the semi-variogram is about 200km. This implies that many observations points (all within a distance of 200km) would measure similar values. Spatial difference on the long run is thus only observed in the Southern part of Limburg and the Veluwe.
Since this kriging model is applied for a long-term average, small spatial differences are filtered out. The snow depth map resulted in a lower RMSE for the kriging model than reported (3.0E−6 compared to 1.1E−1) (Erxleben, et al. 2002). However, for smaller time frames, local variations will have more influence. In that case, it would be better to use Binary Regression trees (Balk, et al. 2000; Erxleben, et al. 2002). However, these studies based their arguments on results achieved in mountainous areas, only one case study was selected in a relatively flat area. It should be researched if the more comprehensive model is truly worth the required data collection.
Remarkable is the overestimation for the used dataset, as the original snow depth data shows a larger variation than the kriged map. More research is required to quantify the interpolation error.
In the SWE validation set, only one weather station is used as validation due to time limitation. For the Barneveldse beek, weather station de Bilt is used. For the Reusel, Eindhoven is set as the reference for the simulated snowfall. It is expected that the validation is more complete if the interpolated map would be used.
All snow depth measurements had to be converted to SWE in order to compare the simulated snowfall and melt. Snow densities were required for this conversion that has not been measured previously in the Netherlands. Literature has been used, but as snow hydrology is mainly researched in colder climates in which significant more snow is fallen. In the work of Egli, et al. (2009), multiple ways of measuring the SWE are described, but in all cases first set up sensors are required, or an extensive dataset to use a stochastic approach. A simple gauge has been used in the Swiss to measure the SWE. This method would be applicable in Dutch lowlands, as KNMI has an extensive network of rain gauges that record precipitation on daily basis. However, for solid precipitation a wind fields have significant influences on the amount of measured snow (Rasmussen, et al. 2010; Wiesinger, 1993; Egli, et al. 2009). Wind blows the solid particles over a rain gauge. This distinct behaviour of snowflakes is studied intensively, and many wind shielded are developed (Fassnacht, 2004; Rasmussen, 2010). Nevertheless, rain observations of KNMI do not have these wind shields. The precipitation under catch may add up to 60% depending on the wind speed (Rasmussen, 2012). Wind speed over $2ms^{-1}$ is enough to cause a significant under catch (Fassnacht, 2004). Without correcting the data, the average observed snow density is 5.4 g cm^{-3} (averaged over 494 days, observed at De Bilt), but the total dataset ranged from 0.8 g cm^{-3} up to 800 g cm^{-3}. Even with a correction, these measurements were not seen as reliable. Commonly used standards apply a range of 100-200 g cm^{-3} for fresh snow, settled snow is more compacted and thus, its density is larger (Meløysund, et al. 2007). Using climate variables, the snow density range is set on 181-377 g cm^{-3} that variety was confirmed by the rare measurements carried out in December 2014 in Wageningen.
Concluding the assumptions for snow density, accurate measurements are required to validate the performance of the melt algorithms. Reviewing the large range of theoretical snow densities, it seems complicated to judge upon accuracy for snowfall and its melt. Hence, the performance of the snow melt algorithms is also determined by the accuracy of the discharge simulation.

3.2. Precipitation separation

"Water balance calculations in cold climates require the separation of precipitation into rain and snow" (Kienzle, 2008:5067). The separation method is often a function of air temperature, although multiple functions of separation are reported. The Dutch (warm) snow conditions are best simulated with the VIC model (see figure 5). This argument is true, if it is assumed that the snow density range of fresh snow is correct. The temperature thresholds are defined upon −0.5℃ – 1.5℃. Even though, daily measurements show that snow falls within a wider range of temperature (−7℃ up to 10.6℃: see figure 18). For the sensitivity research, the majority of snowfall observations (defined on −1.7℃ – 3.7℃) is used to set wider temperature thresholds as an alternative to the standard settings of VIC. This range is slightly larger than the range applied in mountainous areas (Alpes or Andes) (L'Hôte, et al. 2005). He states that regardless climate and altitude similar percentages are applicable for hydrological modelling. Using an extensive dataset, various temperature thresholds have been validated for different mountainous catchments. This dataset verified also the use of the more comprehensive methods (presented in Kienzle, 2008). In our study, the validation set consisted of daily snow depth data solely. Given that, we made an attempt on simulating the snowfall with an adapted gradual model. The underestimation resulting from the VIC model is relatively little compared to the uncertainty in snow density.
The sensitivity analysis shows that wider ranges for snowfall are affecting melt modules. However, they are less sensitive than stated earlier by Loth, et al. (1993). For warm snow conditions, better performances would be achieved using a wide temperature range, since the majority of snow events is fallen in a mixture of snow and rain (KNMI data). Precise meteorological measurements are required to distinguish rain from wet snow, slush or snowflakes. The model of Thériault et al. (2012) gives insight in these transitions, which conversion is crucial for the different phases of precipitation.
Further recommendations would thus be to focus on a precise database, for which accurate simulations can be verified. In addition, the model of Thériault et al. (2012) could be studied further in order to get better view upon the winter precipitation in warm snow conditions.

3.3. Snow melt pre-processors

In the cumulative precipitation plot, it is shown that each melt algorithm simulates a decline in SWE on a different time step. As the total input is defined by the VIC model, which is equal for all algorithms, the timing of melt determines difference between the melt algorithms.
It seems to be that the algorithms are sensitive to different climate factors. The DHF algorithm depends only on temperature and by the DHF factor, the melt per time step can be adjusted. In the SWE plots, it is seen that DHF simulates too much melt at once (winter 2009-2010). In the winter of 2010-2011, the DHF algorithm is not sensitive enough to the temperature increase. The last winter did not show enough difference to distinguish the performance of three algorithms. These contrasting results complicate a real calibration for the melt factor and more snow rich winter should be selected to fine-tune this factor for accurate SWE simulation.

The SRF factor is a semi-empirical method to simulate melt that uses shortwave radiation and the albedo in addition to the temperature index component. Using this physical component, the SRF seems to be less sensitive to a melt factor. In general, the gradual decline corresponds better to the observations, which would imply that the chosen melt factor is in agreement with the observation. Yet again, only two winters can be used to validate the SWE fluctuations. Hence, the SRF melt factor is not calibrated.
In the sensitivity analysis, the input of the global radiation is questioned. Choosing a different location for the Barneveldse beek did not result in a large different for global radiation component of the energy

balance, which would give similar results for the shortwave component in the SRF algorithm.
The constant albedo *is* an important factor to consider, as the albedo normally shows a large variation in time and space (Brock, 2000). Different models exist to simulate the albedo and models are often parameterised on a changing albedo (Marks, et al. 1998; DeWalle and Rango 2011).
Considering a constant albedo, too little reflection would be simulated in case of fresh snow and too much in case of wet (darker) snow. Melt of fresh snow would be overestimated using the two algorithms that contain a global radiation component. The absolute difference is not verified in this study. More research is required to quantify the absolute error by taking a constant albedo.

The energy balance algorithm shows in both winters a sudden depletion of the snow reservoir. This melt event is not observed at the KNMI weather stations, nor observed in the discharge series. The EB algorithm seems to be sensitive to different factors than the two (semi-) empirical algorithms, which is logic reasoning that this algorithm simulates melt physically. Reviewing upon the sensitivity analysis, the algorithm corresponds correctly to cloud cover, as Hock (1999) and Marks, et al. (1998) report similar results.
One large melt event was simulated on December 22nd 2009, which determining fluxes are shown in figure 11. A steep temperature increase is seen in upper graph that increase is reflected by the positive flux of the sensible heat component. In combination with the net radiation and the latent heat flux, a large amount is available for melt that day. In the winter of 2010-2011, a sudden melt peak is simulated once again. This time, the fluxes are not explicitly shown, but the same process takes place. A steep temperature and vapour pressure gradient affects the sensible and latent heat fluxes. The increase of these fluxes changes the sign of the available energy for melt that results in a simulated melt event.
The EB algorithm seems to be sensitive to an increase of warm air temperature, high humidity and large wind speeds. This is confirmed by the study of Marks, et al., (2001). These factors affect the turbulent fluxes. In order to measure the turbulent fluxes accurately, air temperature should be measured at the snowpack surface, while automatic weather stations measure temperature at 1.5m. This may be a large source of error for the energy balance fluxes.
Sensitivity to the height difference of the temperature measurement needs to be researched in detail before implementing the EB algorithm. Due to time limitation, this issue could not be researched in this study. Apparently, the EB algorithm is more sensitive than the observations show. Hence, the error is consistent for the two winters.

3.4. Discharge simulations

For both case studies, a consequent error was visible in the original model simulations compared with the observations. Using snow melt modules, snow surface storage is included in the model and discharge simulations show a delay. In general, the melt algorithms improve the timing of the discharge series. This improvement is reviewed by the cross-correlation that shows stabilized or higher correlations for the melt algorithms. The timing of the melt events is best simulated by the DHF and SRF algorithms. Concluding for the three winters and two catchments, both algorithms indicate an improvement. For two winters only, the results cannot be used to distinguish a ‘best’ fit. All discharge peaks are not simulated perfectly. In general, these peaks are better simulated than using the original model, which is seen by the higher R^2.
Even though, the melt algorithms improved the simulations optically, NSE remained negative for some winters. At the one hand, this source of error can be found in the calibration of the hydrological model, but as reviewed in the previous section, melt events do not correspond entirely with the observations.
The settings of the original hydrological model affect the NSE and R^2. These two methods are sensitive to

a consequent over/under estimations of the discharge series due to the squared variance in their equations (see equations 18+19) (Krause, et al. 2005). In Barneveldse beek, the discharge is systematically overestimated using Sobek. This is reflected for both Sobek models (RR and 1D channel flow). Since the melt algorithms only affect the period with snow, and not the recession simulation, a perfect winter simulation requires some calibration as well as a melt algorithm. The absolute effect of the SRF algorithm is seen best in figure 13. In Reusel, base flows are underestimated using the current settings of WALRUS. The goodness of fit parameters are sensitive to this underestimation, even though the melt peak may be well predicted. The performance of the melt algorithms may be best judged by the cross-correlation scores, as the scale and offset of the time-series is not included in this comparison.

Snowmelt simulations are not optimized yet. The two temperature-index algorithms are not (yet) calibrated to Dutch climate conditions, and the EB algorithm is still too sensitive compared to derived SWE measurements. Spatial differences may play a role, since all climate variables are measured at one automatic weather stations of the KNMI (De Bilt and Eindhoven for catchments Barneveldse beek and Reusel). At the other hand, SWE observations itself show a large uncertainty marge that complicates the fine-tuning of the melt algorithms.
Depending on the desired accuracy, more time will be invested in these snowmelt algorithms. The research' objective of this study is to include snowmelt in the current hydrological models. These hydrological models are used by Water boards. Logically, they will determine the desired accuracy of discharge simulations. If snowfall does not cause major problems annually, it is not so likely that more time and effort is invested in optimizing these algorithms, regardless the current uncertainties in the current simulations.
However, we would stress the necessity of further research to develop the Dutch melt algorithms. Precise SWE measurements enable calibration for the time-index algorithms. Adjusting the melt factor, many uncertainties may be filtered out (Hock, 2003).
In addition, more research is needed to verify the effect of assumptions as a constant albedo and (snow) surface temperature. For the albedo, MODIS images were used in the first phase of the study. However, due to cloudy weather during snow events, these optical images did not provide enough information to include in the algorithms. It may be useful to verify the albedo models to parameterize the changing albedo and thereby, to adjust for the (high) reflection of fresh snow.
Finally, the energy balance seems to be sensitive to temperature gradients. Air temperature is now measured at 1.5m, which may result in higher air temperatures than present at the snowpack surface. This suggestion could not be verified, but reviewing the sensitivity to a temperature increase, it is likely that the EB algorithm simulations will be affected.

5. Conclusions

The aim of this research was to develop a melt algorithm in order to include snowmelt in the current hydrological models. In total, three melt algorithms have been tested. The first algorithm uses an hourly melt factor (DHF) to predict melt depending on air temperature observations. The second algorithm also combines a (different) melt factor with the incoming shortwave radiation and albedo (abbreviated as SRF). The last algorithm simulates the snowpack energy balance (EB), and takes into account the net radiation, sensible heat, latent heat, and the sensible heat of rain fluxes in a snowpack. For three snow-rich winters, two catchments are used to test these melt algorithms. The results are validated by snow depth measurements of the KNMI, and by discharge observations of the case studies.

In general, results show that discharge simulations are improved using melt algorithms. The timing of the discharge peaks is improved in almost all cases, but the estimation of the melt peak is not always correct. The two time-index models meet the observed discharge peaks fairly well without calibration.

Conversely, the energy balance algorithm does not simulate the melt events correctly. This melt algorithm seems to react on a sudden temperature increase, which results in an early melt peak.

Comparing all goodness of fit parameters, snowmelt is best simulated using the time-index model combined with the shortwave radiation component (SFR algorithm). Even though the results are not yet optimized, the timing and peak discharge correspond best with the observations.

6. Recommendations

In general, the functioning of the algorithms can be optimized by an accurate validation set. Snow depth measurements are converted using a theoretical snow density range. The range includes an uncertainty, since snow density is not systematically measured in the Netherlands. Hence, a range of possible SWE is used, but this limits the calibration of the snowmelt algorithms.

Moreover, topics for further research may concern the constant value for the snow albedo that is assumed in this study. The range might be little (0.9-0.65), but the effect can be large. Fresh snowfall reflects almost all shortwave radiation, while wet snow absorbs more radiation. This may change the performance of the snowmelt algorithms positively.

Another topic would be the performance of the energy balance algorithm, which can be improved. Regarding its sensitivity to air temperature, local temperature measurements (close to the snowpack) may improve the melt simulation. In addition, local wind speed and humidity measurements could enhance an accurate simulation of the turbulent fluxes.

7. Literature

Andreadis, K.M. Storck, P. Lettenmaier, D.P. (2009) Modeling snow accumulation and ablation process in forested environments. *Water Resources Research* **45**

Bergström, S. (1995) The HBV model, *Computer models of watershed hydrology, Sing. V.P.* 443-476

Brauer, C.C. Teuling, A.J. Torfs, P.J.J.F. Uijlenhoet, R. (2014a) The Wageningen Lowland Runoff Simulator (WALRUS): a lumped rainfall-runoff model for catchments with shallow groundwater. *Geoscientific model development* **7** 2313-2332

Brauer, C.C. Torfs, P.J.J.F. Teuling, A.J. Uijlenhoet, R. (2014b) The Wageningen Lowland Runoff Simulator (WALRUS): application to the Hupsel Brook catchment and the Cabauw polder. *Hydrological Earth System Sciences* **18** 2313-2332

Brock, B.W. Willis, I.C. Sharp, M.J. (2000) Measurement and parameterization of albedo variations at Haut Glacier d'Arolla, Switzerland *Journal of Glaciology* **46** 155 675–688

Chen, N. Guan, D. Jin, C. Wang, J. Yuan, F. (2011) Influences of snow event on energy balance over temperate meadow in demand season based on eddy covariance measurements. *Journal of Hydrology* **399** 100-107

De Walle, D.R. Rango, A. (2011) Principles of snow hydrology, Cambridge university press, Cambridge, UK, 2008

Dirks, K.N. Hay, J.E. Stow, C.D. Harris, D. (1998) High-resolution studies of rainfall on Norfolk Island. Part II: Interpolation of rainfall data *Journal of Hydrology* **208** 187-193

Egli, L. Jonas, T. Meister, R. (2009) Comparison of different automatic methods for estimating snow water equivalent *Cold Regions Science and Technology* **57** 107-115

Erxleben J, Elder K, Davis R. (2002) Comparison of spatial interpolation methods for estimating snow distribution in the Colorado Rocky Mountains. *Hydrological Processes* **16** 3627–3649

Graysol, R. Bloschl, G. (2001) Spatial Patterns in Catchment Hydrology: Observations and Modelling *CUP* Archive: 404

Groot, S., Versteeg, R., Klopstra, D., Braak, E. van den, Wouters, K., Distributiemodel, deel C, (Noord) Oost en Zuid Nederland, Pr1614.10, april 2009. HKV$_{\text{Lijn in water}}$.

Heijkers, J. Kallen, MJ, Crook, R. (2011) De bouw van de Neerslagdatabank Midden-Nederland. HKV Rapportage in 2011

Hock, R. (1999) A distributed temperature-index ice- and snowmelt model including potential direct solar radiation. *Journal of Glaciology* **45** 101–11

Hock, R. (2003) Temperature index melt modeling in mountain areas *Journal of Hydrology* **282** 104-115

Hock, R. (2014) Energy balance of Snow and Ice *Geophysical Institute, University of Alaska Fairbanks* (unpublished)

Hosang, J Dettwiler, K. (1991) Evaluation of a water equivalent of snow cover map in a small catchment using a geostatistical approach. *Hydrological processes* **5** 283-290

Jungermann, N. Graaff, B. de Kalibratie en gevoeligheidsanalyse District Zuid, NBW-Toetsing district Zuid, PR2492.10, September 2013. $HKV_{\text{Lijn in water}}$.

Kelly, R.E.J. Drake, N.A. Barr, S.L. (2004) Spatial Modelling of the Terrestrial Environment *John Wiley & Sons*

Kienzle, S.W. (2008) A new temperature based method to separate rain and snow, *Hydrological processes* **22** 5067-5085

Klopsta, D. Versteeg, R. (2005) Neerslag afvoer model BOS. Deel 1: Analyse van neerslaggegevens. HKV rapportage PR842.10

KNMI (2000) Handbook of Meteorological observations

Köppen, W. Wegener, A. (1924) Die Klimate der geologischen Vorzeit *Borntreager,* Berlin

Kroes, J.G. Dam, van J.C. Groenendijk, P. Hendriks, R.F.A. Jacobs, C.M.J. (2008) SWAP version 3.2. Theory description and user manual. *Alterra-report* **1649** 262

Kustas, W.P. Rango, A. Uijlenhoet, R. (1994) A simple energy budget algorithm for the snowmelt runoff model. *Water resources research* **30** 5 1515-1527

L' Hote, Y. Chevallier, P. Coudarin, A. Lejeune, Y. Etchevers, P. (2005) Relationship between precipitation phase and air temperature: Comparison between the Bolivian Andes and the Swiss Alpes. *Hydrological Sciences Journal* **50** 987-997

Liang, X. Lettenmaier, D.P. Wood, E.F. Burges, S.J. (1994), A simple hydrologically based model of land surface water and energy fluxes for general circulation models. *Journal Geophysical Research* **99** 14415-14458

Loos, R.E. (2015) Making WALRUS applicable for large catchments: a case study in the Reusel catchment. *MSc Thesis. Wageningen University and Research Centre* (unpublished)

Loth, B. Graf, H-F. Oberhuber, J.M. (1993) Snow Cover Model for Global Climate Simulations. *Journal of geophysical research* **98** D6 10451-10464

Loth, B. Graf, H-F. OberHuber, J.M. (1993) Snow cover model for global climate simulations. *Journal of geophysical Research* **98** 10451-10464

Ly, S. Charles, C. Degré A. (2013) Different methods for spatial interpolation of rainfall data for operational hydrology and hydrological modeling at watershed scale. A review. *Biotechnology, Agronomy, Society and Environment* **17** (2) 392-406.

Marks, D. Kimball, J. Tingey, D. Link, T. (1998) The sensitivity of snowmelt processes to climate conditions and forest cover during rain-on-snow: a case study of the 1996 Pacific Northwest flood. *Hydrological processes* **12** 1569-1587

Marks, D. Link, T. Wintral, A. Garen, D. (2001) Simulating snowmelt processes during rain-on-snow over a semi-arid mountain basin. *Annals of Glaciology* **32**

Matheron G., 1971 *The theory of regionalized variables and its applications*. Paris : École Nationale Supérieure des Mines de Paris.

Nash, J.E. Sutcliffe, J.V. (1970) River flow forecasting through conceptual models, Part I - A discussion of principles. *Journal Hydrology* **10** 282–290

Paterson W.S.B. (1994) The physics of glaciers (third edition). *Oxford: Pergamon Press*, 480 pp

Pellicciotti, F. Brock, B. Strasser, U. Burlando, P. Funk, M. Corripio (2005) An enhanced temperature-index glacier melt model including the shortwave radiation balance: development and testing for Haut Glacier d'Arolla, Switzerland. *Journal of Glaciology* **51** 175 573-587

Petrucci, A. Salvati, N. Seghieri, C. (2003) The application of a Spatial Regression Model to the Analysis and Mapping of poverty. *FAO Sustainable Development, Environment and Natural Resources Service* **7**

Pipes A. Quick M.C. (1977) UBC Watershed model Users Guide. *Department of Civil Engineering*, University of British Columbia: Vancouver, Britisch Columbia, Canada

Prinsen, G. Hakvoort, H. Dahm, R. (2009) Neerslag-afvoermodellering met SOBEK. *Stroming* **16**

Quick, M.C. and Pipes, A. (1976) A combined snowmelt ana rainfall runoff model. Canadian Journal of Civil Engineering **3** 449-460

Salas, J.D. Delleur, J.W. Yevjevich, V. (1980) Applied modeling of hydrological time series. *Water resources Publications*.

Sicart, J.E. Hock, R. Six, D. (2008) Glacier melt, air temperature and energy balance in different climates: The Bolivian Tropics, the French Alps and northern Sweden. *Journal of Geophysical research* **113** D24113

Sturm, M. Holmgren, J. Liston, G.E. (1995) A Seasonal Snow Cover Classification System for Local to Global Applications. *Journal Climate* **8** 1261-1283

Sturm, M. Taras, B. Liston, G.E. Derksen, C. Jonas, T. Lea, J. (2010) Estimating Snow Water Equivalent Using Snow Depth Data and Climate Classes. *Journal of hydrometeorology* **11** 1380-1394

Thériault, J.M. Stewart, R.E. Henson, W. (2012) Impacts of terminal velocity on the trajectory of winter precipitation types *Atmospheric Research* **116** 116-129

Versteeg, R. Hakvoort, H. Bosch, S. Kallen, MJ (2012) Meteobase Online archief van neerslag- en verdampingsgegeven voor het waterbeheer. *Stichting Toegepast Onderzoek Waterbeheer, Stowa* **48** 2

Watson, D.F. Philip, G.M. (1985) A Refinement of Inverse Distance Weighted Interpolation. *Geo-Processing* **2** 315-327

Annex

A.1. Locations of automatic weather stations of the KNMI in the Netherlands

A.2. Locations of manual weather stations of the KNMI in the Netherlands

A.3 Average snow depth in the NL

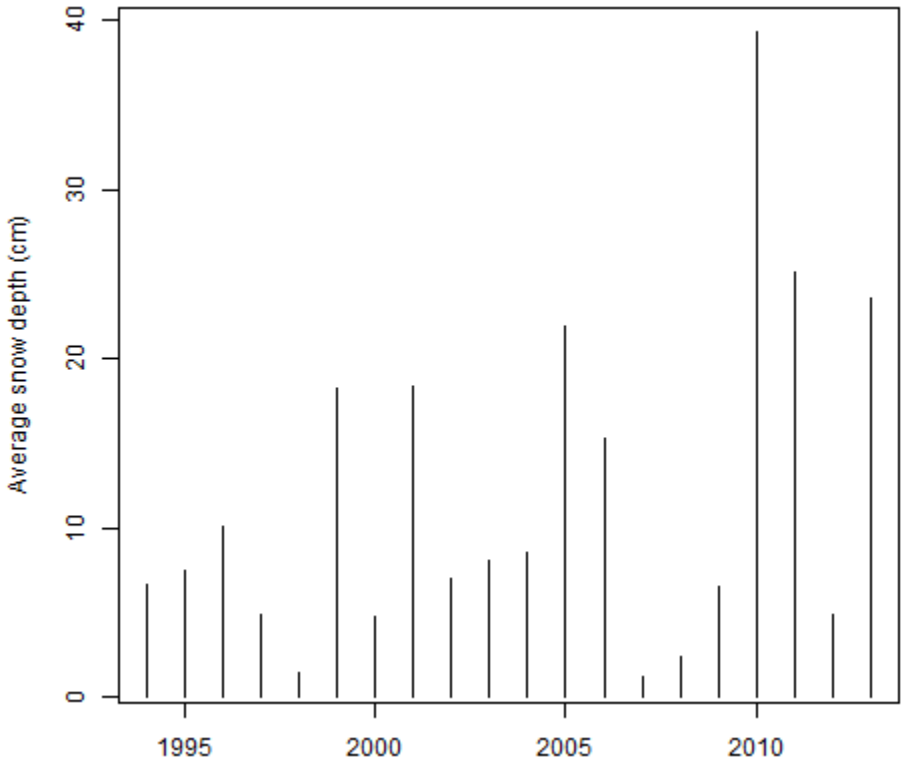

A.4 Experimental Variogram for snow depth measurements of 325 KNMI weather stations

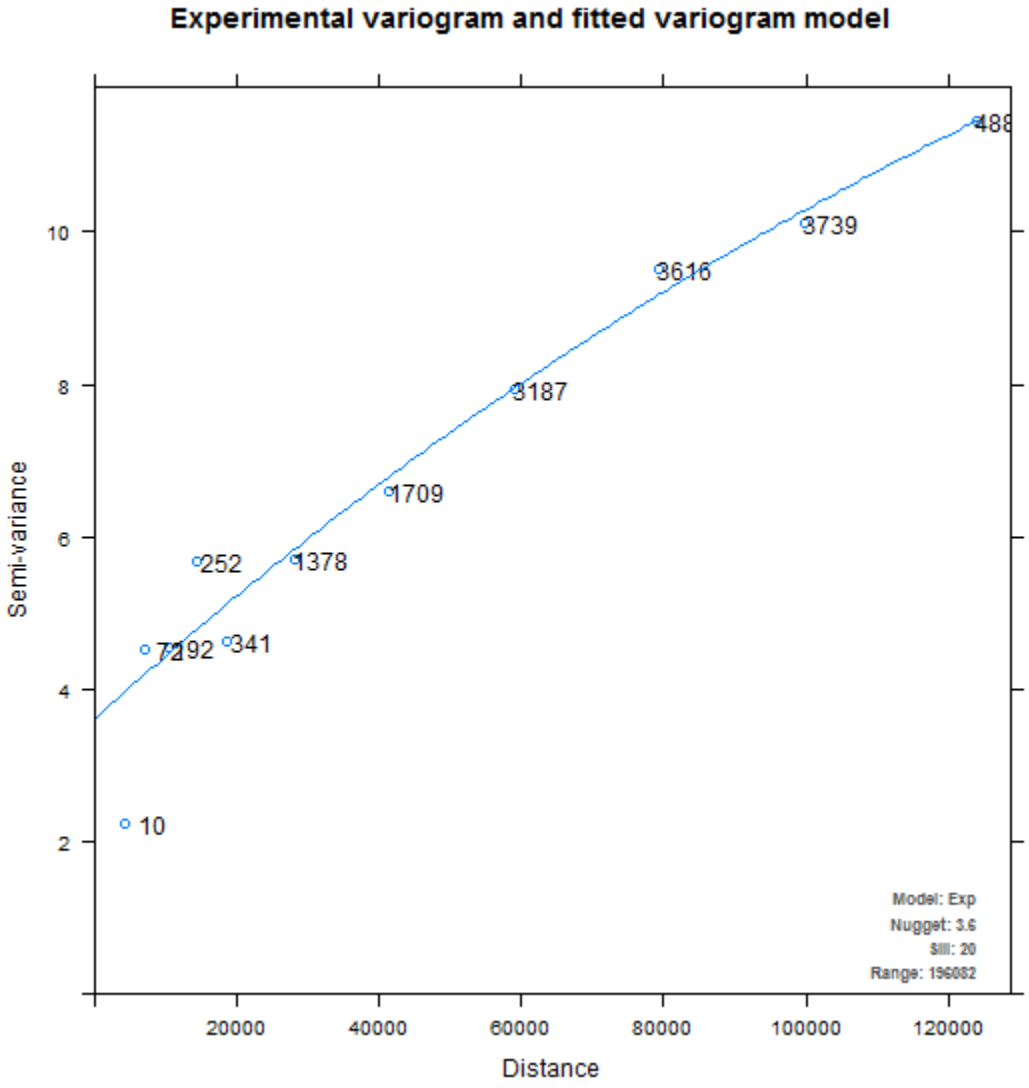

A.5 Average annual Snowfall (cm) for 2005-2014

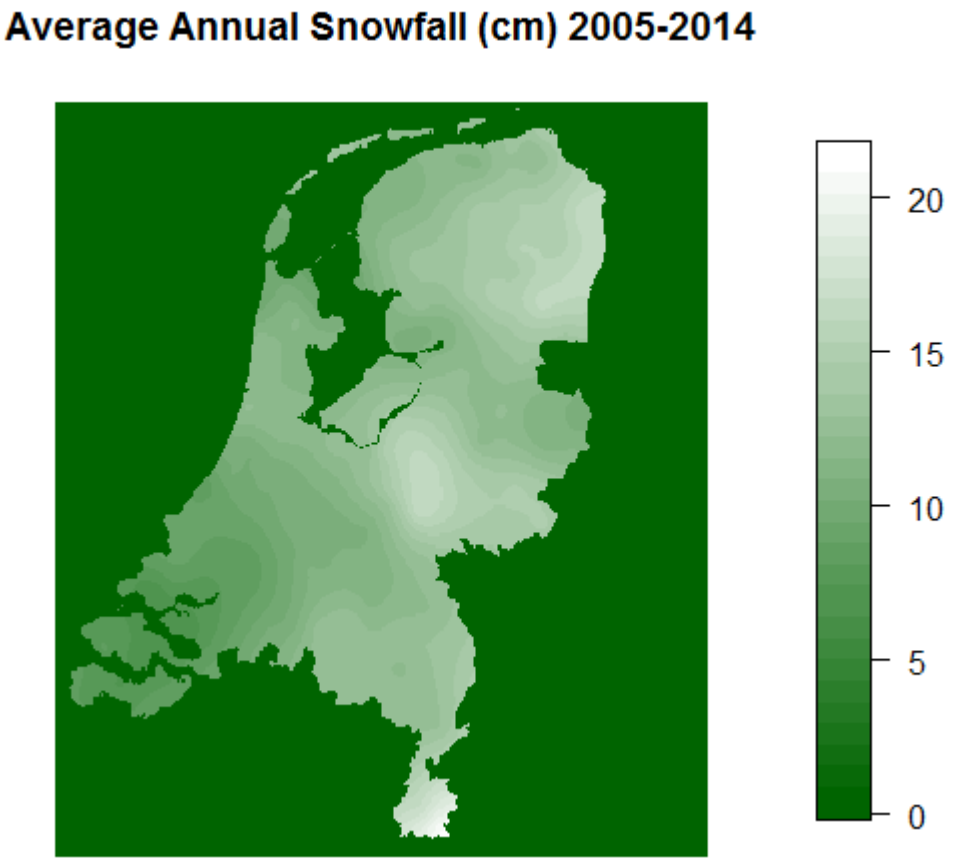

A.6 Snow cover climate regions by Sturm et al. (1998)

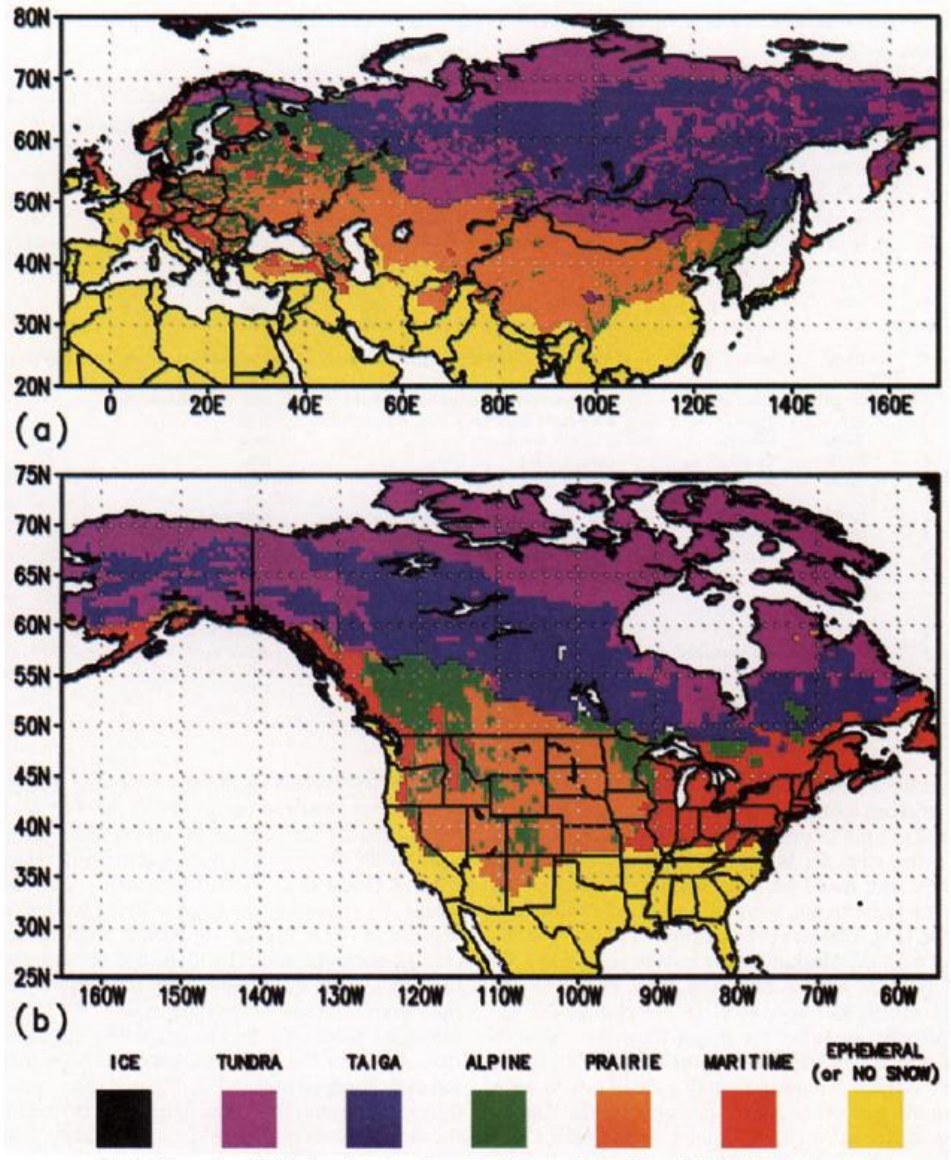

FIG. 10. Snow class distribution based on climate variables in (a) Eurasia and (b) North America.

A.7 Measurements taken in Wageningen 27-12-2014 and 28-12-2014

Table A.7.1: Measured data at 27-12-2014: Cloudy conditions

Location	Weight snow (g)	Weight 1L box (g)	ρ_S (gcm^{-3})
Droef 57	429	50	0.379
Droef 59	461	50	0.411
Bankje	474	56	0.418
Veld 1	478	47	0.431
Veld 2	439	47	0.392
Veld 3	450	47	0.403
Average	455	50	**0.406**

Table A.7.2: Observations at 28-12-2014: Sunny conditions. Some surface hoar is observed at all locations

Location	Weight snow (g)	Weight 1L box (g)	ρ_S (gcm^{-3})
Droef 57	326	54	0.272
Droef 59	331	54	0.277
Bankje	278	54	0.224
Veld 1	300	53	0.247
Veld 2	310	53	0.257
Veld 3	317	53	0.264
Average	310	54	**0.257**

A.8 Cumulative precipitation series in winter 2010-2011

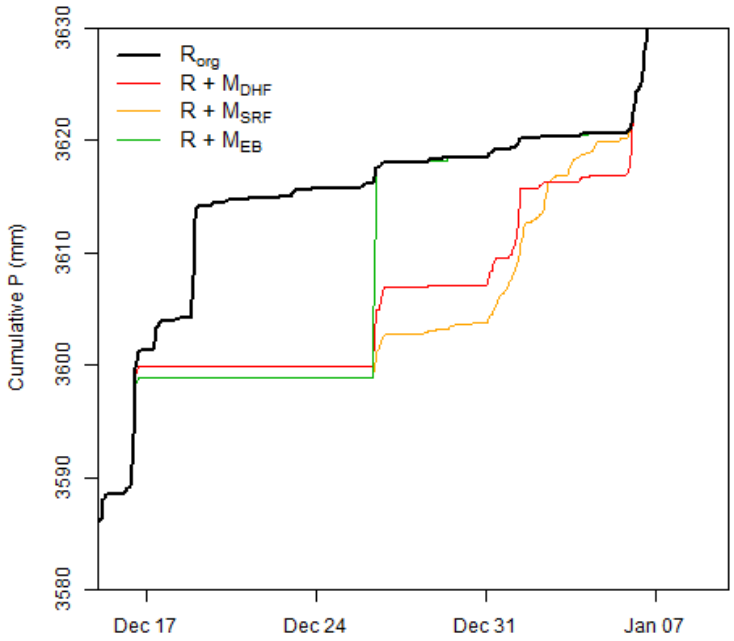

A.9 Cumulative precipitation series in winter 2012

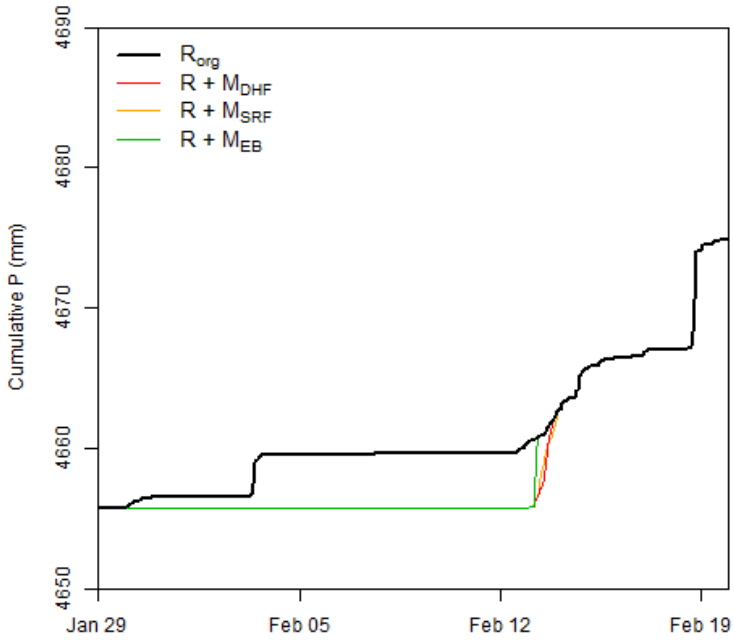

A.10 SWE time series in winter 2010-2011

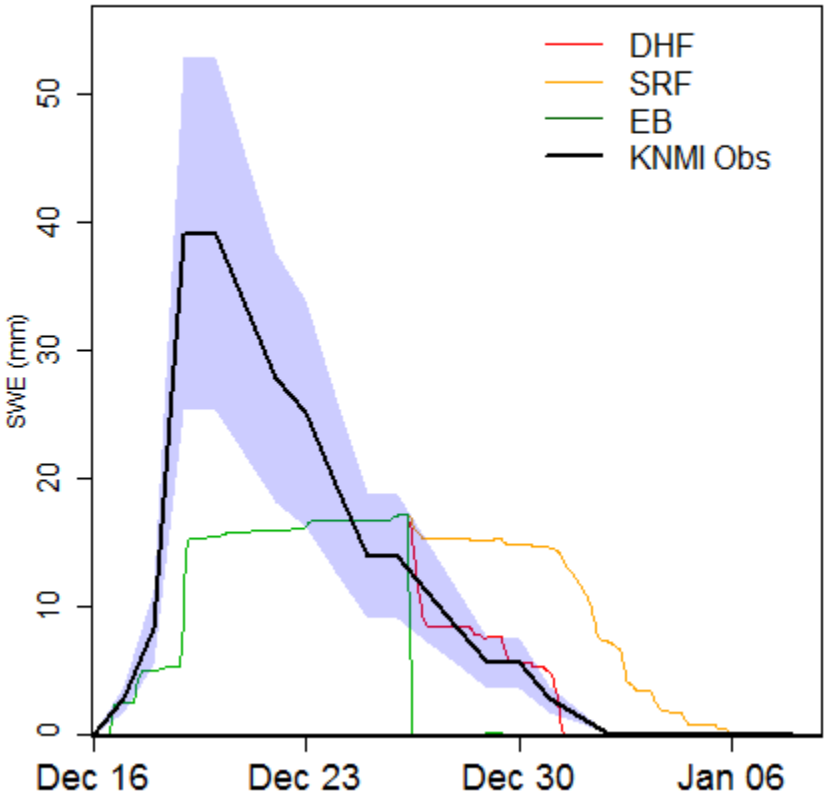

A.11 SWE time series in winter 2012

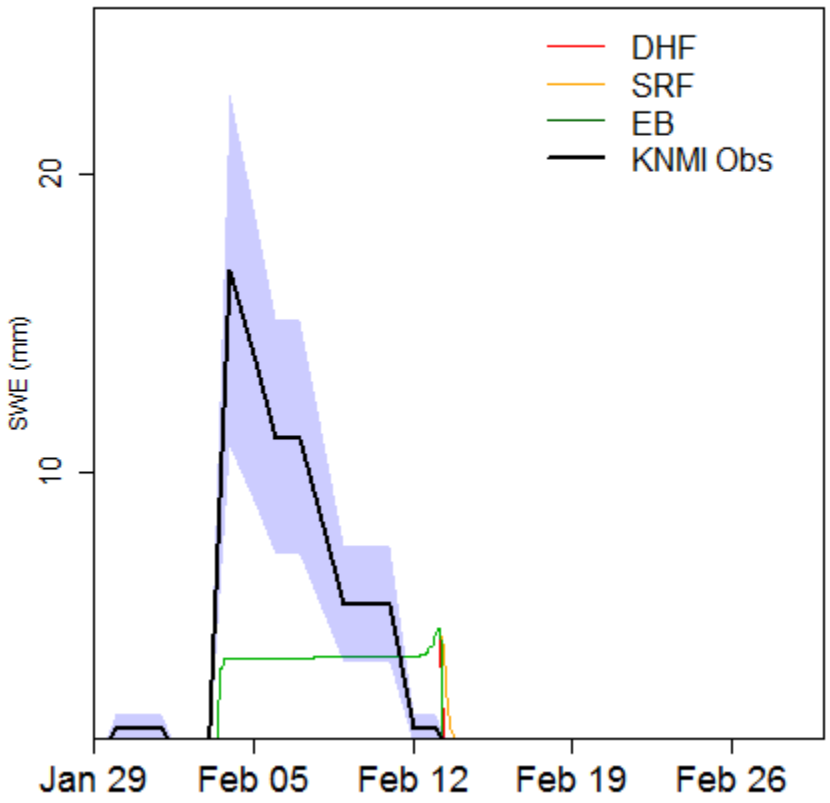

A.12 Discharge simulations for the Barneveldse beek using Sobek: results for the winter of 2010-2011

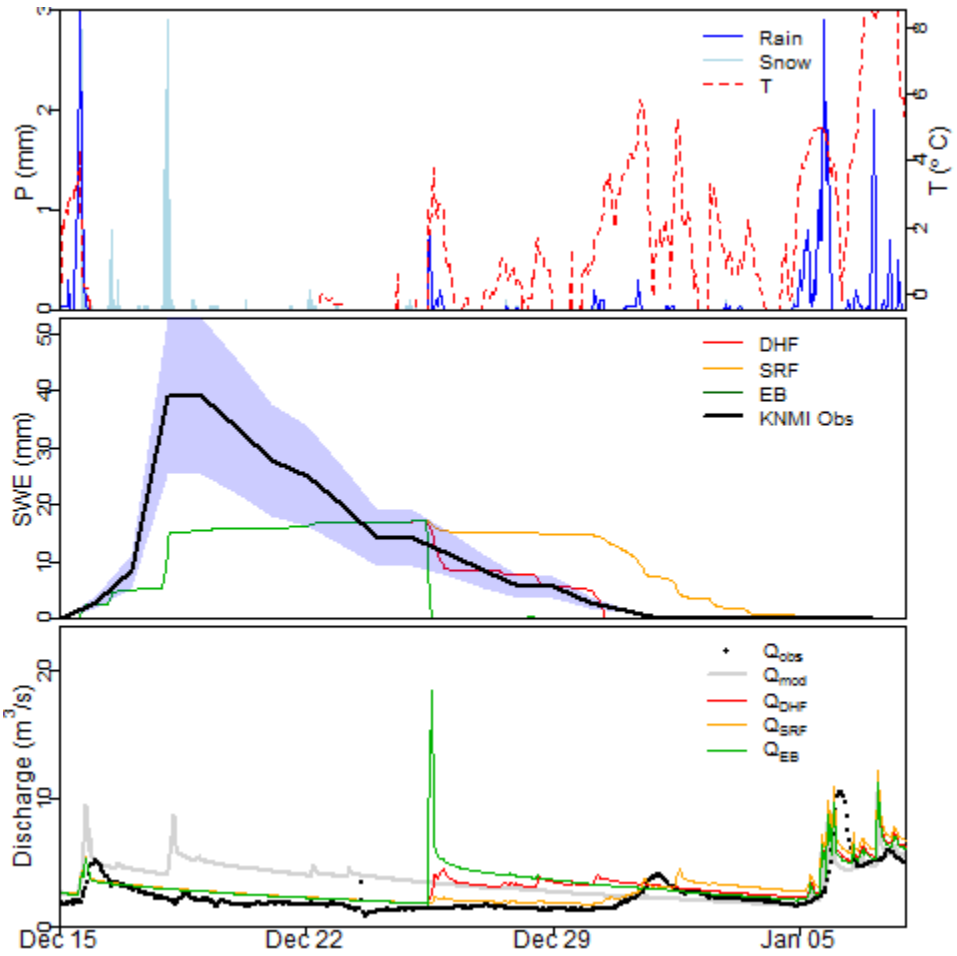

Figure A.1221: Discharge simulation of Barneveldse beek in the winter of 2011. In the first plot the separated precipitation and temperature are seen. The second plot shows the simulated SWE and its decrease, in addition the recorded KNMI values (with an uncertainty range: shaded area) are displayed. In the last plot the simulated discharge is shown for all models (incl. original in grey) together with the observations (dotted line).

A.13 Discharge simulations for the Barneveldse beek using Sobek: results for the winter of 2012

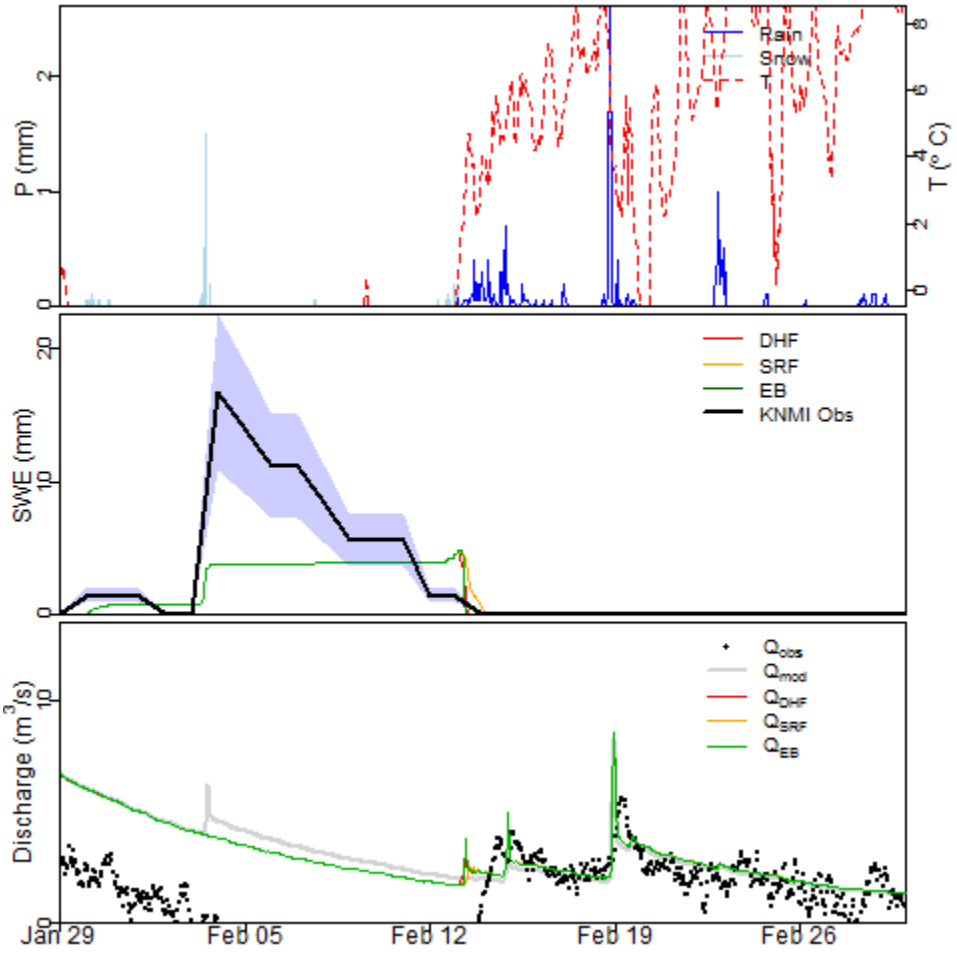

Figure A.13: Discharge simulation of Barneveldse beek in the winter of 2011. In the first plot the separated precipitation and temperature are seen. The second plot shows the simulated SWE and its decrease, in addition the recorded KNMI values (with an uncertainty range: shaded area) are displayed. In the last plot the simulated discharge is shown for all models (incl. original in grey) together with the observations (dotted line).

A.14 Cumulative precipitation time series for weather station in Eindhoven